Single-Carrier Modulation versus OFDM for Millimeter-Wave Wireless MIMO

# Single-Carrier Modulation versus OFDM for Millimeter-Wave Wireless MIMO

Stefano Buzzi, *Senior Member*, *IEEE*, Carmen D'Andrea, Tommaso Foggi, Alessandro Ugolini, and Giulio Colavolpe, *Senior Member*

**Abstract**

Future wireless networks will extensively rely upon carrier frequencies larger than 10 GHz. Indeed, recent research has shown that, despite the large path-loss, millimeter wave (mmWave) frequencies can be successfully exploited to transmit very large data-rates over short distances to slowly moving users. This paper presents results on the achievable spectral efficiency on a wireless MIMO link operating at mmWave in a typical 5G scenario. Two different single-carrier modem schemes are considered, i.e., a traditional modulation scheme with linear equalization at the receiver, and a single-carrier modulation with cyclic prefix, frequency-domain equalization and FFT-based processing at the receiver; these two schemes are compared with a conventional MIMO-OFDM transceiver structure. Our analysis takes into account the peculiar characteristics of MIMO channels at mmWave frequencies, the use of hybrid (analog-digital) pre-coding and post-coding beamformers, and the finite cardinality of the modulation structure. Our results show that the best performance is achieved by single-carrier modulation with time-domain equalization, while MIMO-OFDM performs slightly better than single carrier modulation with frequency-domain equalization. Results also confirm that the spectral efficiency increases with the dimension of the antenna array, as well as that performance gets severely degraded when the link length exceeds 90-100 meters and the transmit power falls below 0 dBW.

**Index Terms**

S. Buzzi and C. D'Andrea are with the Department of Electrical and Information Engineering, University of Cassino and Lazio Meridionale, I-03043 Cassino, Italy ({buzzi, carmen.dandrea}@unicas.it).

T. Foggi, A. Ugolini and G. Colavolpe are with the Department of Information Engineering, University of Parma, I-43100 Parma, Italy (tommaso.foggi@nemo.unipr.it, {alessandro.ugolini, giulio}@unipr.it).

This paper was partly presented at the 20th International ITG Workshop on Smart Antennas, Munich, Germany, March 2016.

mmWave, 5G, MIMO, single-carrier modulation, spectral efficiency, MIMO-OFDM, time-domain equalization, frequency-domain equalization, hybrid decoding.

## I. Introduction

The use of carrier frequencies larger than 10 GHz will be one of the main new features of fifth-generation (5G) wireless networks [1], and, due to the availability of large and currently unused bandwidths, will be instrumental in delivering gigabit data-rates per users. Until few years ago, the use of mmWave frequencies for cellular communications had been neglected due to the higher atmospheric absorption that they suffer compared to other frequency bands and to the larger values of the free-space path-loss. However, recent measurements suggest that mmWave attenuation is only slightly worse than in other bands, as far as propagation in dense urban environments and over short distances (up to about 100 meters) is concerned [2]. Additionally, since antennas at these wavelengths are very small, arrays with several elements can be packed in small volumes, in principle also on mobile devices, thus removing the traditional constraint that only few antennas can be placed on a smartphone and benefiting of an array gain at both edges of the communication link with respect to traditional cellular links. A large body of work has been recently carried out on the use of mmWave frequencies for cellular communications [2]–[6]. Nowadays, several prototypes and test-beds showing the potentiality of mmWave frequencies for cellular applications are already available [7] and the EU-funded project 5G-CHAMPION is planning a large scale demo for the 2018 Winter Olympic Games in Seoul (Republic of Korea) at 28 GHz frequency.

One of the key questions about the use of mmWave frequencies and in general about 5G cellular systems is about the type of modulation that will be used at these frequencies. Indeed, while it is not even sure that 5G systems will use orthogonal frequency division multiplexing (OFDM) modulation at classical cellular frequencies [8], there are reasons that push for 5G networks operating a single-carrier modulation (SCM) at mmWave frequencies [2]. First of all, the propagation attenuation of mmWave frequencies makes them a viable technology only for small-cell, dense networks, where few users will be associated to any given base station, thus implying that the efficient frequency-multiplexing features of OFDM may not be really needed. Additionally, the large bandwidth would cause low OFDM symbol duration, which, coupled with small propagation delays, means that the users may be multiplexed in the time domain as efficiently as in the frequency domain. Finally, mmWave frequencies will be operated together with massive antenna arrays to overcome propagation attenuation. This makes digital beamforming unfeasible, since the energy required for digital-to-analog and analog-to-digital conversion would be huge. Thus, each user will have an own radio-frequency beamforming, which requires users to be separated in time rather than frequency. For efficient removal of the intersymbol interference induced by the frequency-selective nature of the channel, the use of SCM coupled with a cyclic prefix has been proposed, so that FFT-based processing might be performed at the receiver [9]. In [10], [11], the null cyclic prefix single carrier (NCP-SC) scheme has been proposed for mmWave frequencies. The concept is to transmit a single-carrier signal, in which the usual cyclic prefix used by OFDM is replaced by nulls appended at the end of each transmit symbol. Given the cited prohibitive hardware complexity of fully-digital (FD) beamforming structures, several mmWave-specific MIMO architectures have been proposed, where signal processing is accomplished in a mixture of analog and digital domains (see, for instance, [12] and references therein). In particular, while FD beamforming requires one RF chain for each antenna, in hybrid structures a reduced number of RF chains is used, and beamforming is made partially in the digital domain and partially at RF frequencies, where only the signal phase (and not the amplitude) can be tuned prior to antenna trasmission.

This paper is concerned with the evaluation of the achievable spectral efficiency (ASE) of SCM schemes operating over MIMO links at mmWave frequencies. We consider three possible transceiver architectures: (a) SCM with linear minimum mean square error (LMMSE) equalization in the time domain for intersymbol interference removal and symbol-by-symbol detection; (b) SCM with cyclic prefix and FFT-based processing and LMMSE equalization in the frequency domain at the receiver; and (c) plain MIMO-OFDM architecture for benchmarking purposes. The ASE is computed by using the simulation-based technique for computing information-rates reported in [13]; this technique, that has been already used in several other cases [14], [15], permits taking into account the finite cardinality of the modulation, and thus provides more accurate results than the ones that are usually reported in the literature and that refer to Gaussian signaling. The considered transceiver structures use hybrid pre-coding and post-coding beamforming structures, with a number of RF chains equal to the used multiplexing order - this is indeed the minimum possible number of RF chains and so the resulting structures are the one with the lowest complexity. We also provide an analysis of the system bit-error-

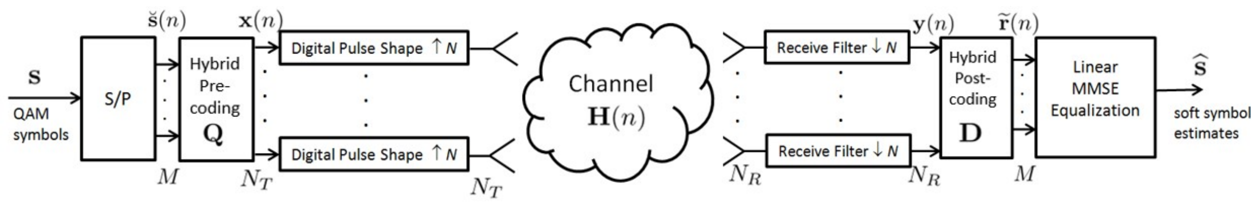


Figure 1. Transceiver block-scheme for SCM with TDE.

rate (BER), under the assumption that low-density parity-check (LDPC) codes are used. Our results will show that, among the three considered transceiver schemes, SCM with time-domain equalization (SCM-TDM) achieves by far the best performance, while MIMO-OFDM is only slightly better than SCM with frequency-domain equalization (SCM-FDE). Moreover, our results provide a further confirmation of the fact that for distances up to 100 meters, and with a transmit power around 0 dBW, mmWave links exhibit a very good performance and may be very useful in wireless cellular applications; for larger distances instead, either larger values of the transmit power or a larger number of antennas must be employed to overcome the distance-dependent increased attenuation.

The rest of this paper is organized as follows. Next Section contains the system model, with details on the considered mmWave channel model and on the front-end transmitter and receiver. In Section III the three considered transceiver structures, namely SCM-TDE, SCM-FDE and MIMO-OFDM, are accurately described, while the design of the hybrid pre-coding and post-coding beamforming structures is reported in Section IV. Extensive numerical results on the system ASE and on the coded BER are illustrated and discussed in Section V, while, finally, Section VI contains concluding remarks.

*Notation:* The symbol $(\cdot)^H$ denotes conjugate transpose, $(\cdot)^T$ denotes transpose, and $\mathbf{I}_N$ denotes the $(N \times N)$-dimensional identity matrix. The symbol $\circledast$ denotes circular convolution, $\mathrm{E}[\cdot]$ denotes expectation, while, finally, $\|\cdot\|_{\mathrm{F}}$ denotes the Frobenius norm.

## II. System model

We consider a transmitter-receiver pair that may be representative of either the uplink or the downlink of a cellular system. We denote by $N_T$ and $N_R$ the number of transmit and receive antennas, respectively, and consider the general case of a frequency-selective channel.

### A. The channel model

The propagation channel can be modeled as an $(N_R \times N_T)$-dimensional matrix-valued continuous time function, that we denote by $\mathbf{H}(t)$. According to the popular clustered model for MIMO mmWave channels, we assume that the propagation environment is made of $N_{\rm cl}$ scattering clusters, each of which contributes with $N_{{\rm ray},i}$ propagation paths $i = 1, \ldots, N_{\rm cl}$, plus a possibly present LOS component. We denote by $\phi^r_{i,l}$ and $\phi^t_{i,l}$ the azimuth angles of arrival and departure of the $l^{th}$ ray in the $i^{th}$ scattering cluster, respectively; similarly, $\theta^r_{i,l}$ and $\theta^t_{i,l}$ are the elevation angles of arrival and departure of the $l^{th}$ ray in the $i^{th}$ scattering cluster, respectively. Denoting by $h_{\rm TX}(t)$ the baseband equivalent transmit shaping filters,[1] by $h_{\rm RX}(t)$ the baseband equivalent of the impulse response of the $N_R$ receive filters, and by $h(t) = h_{\rm TX}(t) * h_{\rm RX}(t)$ their convolution, and assuming a sampling interval equal to $T_s$, the impulse-response of the linear time-invariant system consisting of the $N_T$ transmit shaping filters, the propagation channel, and the $N_R$ receive filters is a matrix-valued (of dimension $N_R \times N_T$) discrete-time sequence that can be written as follows:

$$\widetilde{\mathbf{H}}(n) \quad = \quad \gamma \sum_{i=1}^{N_{\rm cl}} \sum_{l=1}^{N_{{\rm ray},i}} \alpha_{i,l} \sqrt{L(r_{i,l})} \mathbf{a}_r(\phi^r_{i,l}, \theta^r_{i,l}) \mathbf{a}_t^H(\phi^t_{i,l}, \theta^t_{i,l}) h(nT_s - \tau_{i,l}) + \widetilde{\mathbf{H}}_{\rm LOS}(n) \quad . \quad (1)$$

In the above equation, $\alpha_{i,l}$ and $L(r_{i,l})$ are the complex path gain and the attenuation associated to the $(i,l)$-th propagation path (whose length is denoted by $r_{i,l}$), respectively; $\tau_{i,l} = r_{i,l}/c$, with $c$ the speed of light, is the propagation delay associated with the $(i,l)$-th path. The complex gain $\alpha_{i,l} \sim \mathcal{CN}(0, \sigma^2_{\alpha,i})$, with $\sigma^2_{\alpha,i} = 1$ [16]. The factors $\mathbf{a}_r(\phi^r_{i,l}, \theta^r_{i,l})$ and $\mathbf{a}_t(\phi^t_{i,l}, \theta^t_{i,l})$ represent the normalized receive and transmit array response vectors evaluated at the corresponding angles of arrival and departure; additionally, $\gamma = \sqrt{\dfrac{N_R N_T}{\sum_{i=1}^{N_{\rm cl}} N_{{\rm ray},i}}}$ is a normalization factor ensuring that the received signal power scales linearly with the product $N_R N_T$. Regarding the array response vectors $\mathbf{a}_r(\phi^r_{i,l}, \theta^r_{i,l})$ and $\mathbf{a}_t(\phi^t_{i,l}, \theta^t_{i,l})$, a planar antenna array configuration is used for the transmitter and receiver, with $Y_r$, $Z_r$ and $Y_t$, $Z_t$ antennas respectively on the horizontal and vertical axes for the receiver and for the transmitter. Letting $k = 2\pi/\lambda$, $\lambda$ the considered

[1]We have $N_T$ of such filters.

wavelength, and denoting by $\tilde{d}$ the inter-element spacing we have

$$\mathbf{a}_x(\phi_{i,l}^x, \theta_{i,l}^x) = \frac{1}{\sqrt{Y_x Z_x}}[1, \ldots, e^{-jk\tilde{d}(m \sin\phi_{i,l}^x \sin\theta_{i,l}^x + n\cos\theta_{i,l}^x)}, \\ \ldots, e^{-jk\tilde{d}((Y_x-1)\sin\phi_{i,l}^x \sin\theta_{i,l}^x + (Z_x-1)\cos\theta_{i,l}^x)}] ,$$

where $x$ may be either $r$ or $t$. Let us now comment on the LOS component $\widetilde{\mathbf{H}}_{\mathrm{LOS}}(n)$ in (1). Denoting by $\phi_{\mathrm{LOS}}^r$, $\phi_{\mathrm{LOS}}^t$, $\theta_{\mathrm{LOS}}^r$, and $\theta_{\mathrm{LOS}}^t$ the departure angles corresponding to the LOS link, we assume that

$$\mathbf{H}_{\mathrm{LOS}}(n) = I_{\mathrm{LOS}}(d)\sqrt{N_R N_T} e^{j\eta}\sqrt{L(d)}\mathbf{a}_r(\phi_{\mathrm{LOS}}^r, \theta_{\mathrm{LOS}}^r)\mathbf{a}_t^H(\phi_{\mathrm{LOS}}^t, \theta_{\mathrm{LOS}}^t)h(nT_s - \tau_{\mathrm{LOS}}) . \tag{2}$$

In the above equation, $\eta \sim \mathcal{U}(0, 2\pi)$, while $I_{\mathrm{LOS}}(d)$ is an indicator function/Bernoulli random variable, equal to 1 if a LOS link exists between transmitter and receiver. We refer the reader to [17] for a complete specification of all the channel parameters needed to describe the channel model in (1). Assuming that the multipath delay spread spans $P$ sampling intervals and that the duration of the transmit and receive shaping filters spans $P_h$ sampling intervals each, it is easily seen that the matrix-valued channel sequence $\widetilde{\mathbf{H}}(n)$ has $\widetilde{P} = P + 2P_h - 1$ non-zero elements; for ease of notation, we assume, as usually happens, that the non-zero elements of $\widetilde{\mathbf{H}}(n)$ are those corresponding to $n = 0, \ldots, \widetilde{P} - 1$.

### *B. Input-output relation*

Denoting by $\mathbf{x}(n)$ the $N_T$-dimensional vector to be transmitted at discrete epoch $n$, it is easily shown that the received discrete-time signal at the output of the receive shaping filters is represented by the following $N_R$-dimensional vector

$$\mathbf{y}(n) = \sum_{\ell=0}^{\widetilde{P}-1} \widetilde{\mathbf{H}}(\ell)\mathbf{x}(n-\ell) + \mathbf{w}(n) , \tag{3}$$

with $\mathbf{w}(n)$ denoting the $N_R$-dimensional thermal noise vector at the output of the receive shaping filters. It is seen from (3) that the input-output relationship introduces intersymbol interference (ISI), thus implying that for SCM schemes properly equalization structures will be needed. Regarding the additive thermal noise, it is uncorrelated across antennas, i.e., the noise samples collected through different receive antennas are statistically independent: the vector $\mathbf{w}(n)$ is thus a complex zero-mean Gaussian random variable with covariance matrix $\sigma_w^2 \mathbf{I}_{N_R}$, with $\sigma_w^2 =$

$2\mathcal{N}_0 \int_{-\infty}^{+\infty} |h_{\mathrm{RX}}(t)|^2 \mathrm{d}t$. Conversely, noise samples are in general correlated through time, i.e., we have

$$E\left[w_i(n) w_i^*(n-l)\right] = 2\mathcal{N}_0 r_{h_{\mathrm{RX}}}(lT_s) \ , \tag{4}$$

$\forall i = 1, \ldots, N_R$, where $w_i(n)$ denotes the $i$-th entry of the vector $\mathbf{w}(n)$, and $r_{h_{\mathrm{RX}}}(\tau) = \int_{-\infty}^{+\infty} h_{\mathrm{RX}}(t) h_{\mathrm{RX}}^*(t-\tau) \mathrm{d}t$ denotes the correlation function of the receive shaping filter. It thus follows that, if we arrange $L$ consecutive noise vectors in an $(N_R \times L)$-dimensional matrix

$$\mathbf{W} = \left[\mathbf{w}(n)\ \mathbf{w}(n-1)\ \ldots, \mathbf{w}(n-L+1)\right] \ ,$$

we have that the entries of the matrix $\mathbf{W}$ are vertically uncorrelated (actually, independent) and horizontally correlated.

## III. Transceiver processing

Denote now by s a column vector containing the $L$ data-symbols – drawn either from a QAM constellation or from a Gaussian distribution, and with average energy $P_T$ – to be transmitted:

$$\mathbf{s} = \left[s_0, s_1, \ldots, s_{L-1}\right]^T \ . \tag{5}$$

We assume that $L = kM$, where $k$ is an integer and $M$, the multiplexing order, is the number of information symbols that are simultaneously transmitted by the $N_T$ transmit antennas in each symbol interval. In the following, we present three possible transceiver models.

### *A. SCM with TDE*

We refer to the discrete-time block-scheme reported in Fig. 1. The QAM symbols in vector s are fed to a serial-to-parallel (S/P) conversion block that splits them in $k$ distinct $M$-dimensional vectors $\breve{\mathbf{s}}(1), \ldots, \breve{\mathbf{s}}(k)$. These vectors are pre-coded using the $(N_T \times M)$-dimensional precoding matrix $\mathbf{Q}$; we thus obtain the $N_T$-dimensional vectors

$$\mathbf{x}(n) = \mathbf{Q}\breve{\mathbf{s}}(n) \ , \qquad n = 1, \ldots, k \ .$$

The vectors $\mathbf{x}(n)$ are fed to a bank of $N_T$ identical shaping filters, converted to RF and transmitted.

At the receiver, after baseband-conversion, the $N_R$ received signals are passed through a bank of filters matched to those used for transmission and sampled at symbol-rate. We thus obtain the

$N_R$-dimensional vectors $\mathbf{y}(n)$, which are passed through a postcoding matrix, that we denote by $\mathbf{D}$, of dimensions $(N_R \times M)$. Recalling that $\widetilde{\mathbf{H}}(n)$ is the matrix-valued FIR filter representing the composite channel impulse response (i.e., the convolution of the transmit filter, actual matrix-valued channel, and receive filter) it is easy to show, by virtue of the input-output relationship (3) that the generic $M$-dimensional vector at the output of the postcoding matrix, say $\widetilde{\mathbf{r}}(n)$, is written as

$$\widetilde{\mathbf{r}}(n) = \mathbf{D}^H \mathbf{y}(n) = \sum_{\ell=0}^{\widetilde{P}-1} \mathbf{D}^H \widetilde{\mathbf{H}}(\ell) \mathbf{Q} \breve{\mathbf{s}}(n-\ell) + \mathbf{D}^H \mathbf{w}(n) \ . \tag{6}$$

So far, the choice of the pre-coding and post-coding beamforming matrices $\mathbf{Q}$ and $\mathbf{D}$ has been left unspecified. Since, as already said, FD structures are not practically realizable for mobile wireless applications due to hardware complexity and energy consumption issues, in this paper we will consider reduced-complexity hybrid analog-digital beamforming structures in order to approximate the desired FD beamforming strategies. In the following, we describe the considered FD beamforming structures, leaving to the next section the exposition of the algorithms for the design of the hybrid structures. Letting $\eta = \arg\max_{\ell=0,\ldots,\widetilde{P}-1} \left\{ \left\| \widetilde{\mathbf{H}}(\ell) \right\|_{\mathrm{F}} \right\}$, we assume here that $\mathbf{Q}$ contains on its columns the left eigenvectors of the matrix $\widetilde{\mathbf{H}}(\eta)$ corresponding to the $M$ largest eigenvalues, and that the matrix $\mathbf{D}$ contains on its columns the corresponding right eigenvectors. Note that, due to the presence of ISI, the proposed pre-coding and post-coding structures are not optimal. Nevertheless, we make here this choice for the sake of simplicity, and resort to the use of an equalizer to cancel the effects of ISI. We will adopt a linear minimum mean square error (LMMSE) equalizer making a block processing of $\widetilde{P}$ consecutive received data vectors: to obtain a soft estimate of the data vector $\breve{\mathbf{s}}(n)$, the $\widetilde{P}$ observables $\widetilde{\mathbf{r}}(n+\widetilde{P}-1) \ldots \widetilde{\mathbf{r}}(n)$ are stacked into a single $\widetilde{P}M$-dimensional vector, that we denote by $\widetilde{\mathbf{r}}_{\widetilde{P}}(n)$:

$$\widetilde{\mathbf{r}}_{\widetilde{P}}(n) = [\widetilde{\mathbf{r}}(n+\widetilde{P}-1) \ldots \widetilde{\mathbf{r}}(n)]^T \ .$$

Through ordinary algebra, it is easy to recognize that this vector can be expressed in the form

$$\widetilde{\mathbf{r}}_{\widetilde{P}}(n) = \mathbf{A} \widetilde{\mathbf{s}}_{\widetilde{P}}(n) + \mathbf{B} \widetilde{\mathbf{w}}_{\widetilde{P}}(n) \ , \tag{7}$$

where $\widetilde{\mathbf{s}}_{\widetilde{P}}(n)$ is an $M(2\widetilde{P}-1)$-dimensional vector containing the data symbols contributing to $\widetilde{\mathbf{r}}_{\widetilde{P}}(n)$, i.e.:

$$\breve{\mathbf{s}}_{\widetilde{P}}(n) = [\breve{\mathbf{s}}(n+\widetilde{P}-1) \ldots \breve{\mathbf{s}}(n) \ldots \breve{\mathbf{s}}(n-\widetilde{P}+1)]^T \ , \tag{8}$$

$\widetilde{\mathbf{w}}_{\widetilde{P}}(n)$ is the following $N_R\widetilde{P}$-dimensional noise vector

$$\widetilde{\mathbf{w}}_{\widetilde{P}}(n) = [\widetilde{\mathbf{w}}(n+\widetilde{P}-1)\ldots\widetilde{\mathbf{w}}(n)]^T \ , \tag{9}$$

and $\mathbf{A}$ and $\mathbf{B}$ are suitable matrices, of dimension $[M\widetilde{P} \times M(2\widetilde{P}-1)]$ and $[M\widetilde{P} \times N_R\widetilde{P}]$, respectively. The LMMSE estimator of the desired data vector $\widehat{\mathbf{s}}(n)$ is obtained through the following processing:

$$\widehat{\check{\mathbf{s}}}(n) = \mathbf{E}^H\widetilde{\mathbf{r}}_{\widetilde{P}}(n) \ , \tag{10}$$

where $\mathbf{E}$ is the $(\widetilde{P}M \times M)$-dimensional matrix LMMSE estimator. Its expression is given by [18]:

$$\mathbf{E} = (E[\widetilde{\mathbf{r}}_{\widetilde{P}}(n)\widetilde{\mathbf{r}}_{\widetilde{P}}(n)^H])^{-1}E[\widetilde{\mathbf{r}}_{\widetilde{P}}(n)\check{\mathbf{s}}(n)^H] \ , \tag{11}$$

where

$$\begin{aligned} E[\widetilde{\mathbf{r}}_{\widetilde{P}}(n)\widetilde{\mathbf{r}}_{\widetilde{P}}(n)^H] &= \tfrac{P_T}{M}\mathbf{A}\mathbf{A}^H + \mathbf{B}\mathbf{C}_{\widetilde{\mathbf{w}}_{\widetilde{\mathbf{P}}}}\mathbf{B}^H \ , \\ E[\widetilde{\mathbf{r}}_{\widetilde{P}}(n)\check{\mathbf{s}}(n)^H] &= \ \tfrac{P_T}{M}\mathbf{A}\mathbf{G}_{\widetilde{P}} \ . \end{aligned} \tag{12}$$

In (12), $\mathbf{C}_{\widetilde{\mathbf{w}}_{\widetilde{\mathbf{P}}}} = E[\widetilde{\mathbf{w}}_{\widetilde{P}}(n)\widetilde{\mathbf{w}}_{\widetilde{P}}^H(n)]$ is the covariance matrix of the noise vector $\widetilde{\mathbf{w}}_{\widetilde{P}}(n)$, while $\mathbf{G}_{\widetilde{P}}$ is an $[M \times M(2\widetilde{P}-1)]$-dimensional matrix defined as follows::

$$\mathbf{G}_{\widetilde{P}} = \begin{bmatrix} \mathbf{0}_{[M\times M(\widetilde{P}-1)]} & \mathbf{I}_M & \mathbf{0}_{[M\times M(\widetilde{P}-1)]} \end{bmatrix}^T \ . \tag{13}$$

*Considerations on complexity.* Regarding processing complexity, we note that the computation of the equalization matrix $\mathbf{E}$ requires the inversion of the covariance matrix of the vector $\widetilde{\mathbf{r}}_{\widetilde{P}}(n)$, with a computational burden proportional to $(\widetilde{P}M)^3$; then, implementing (10) requires a matrix vector product, with a computational burden proportional to $(\widetilde{P}M^2)$; this latter task must be made $k$ times in order to provide the soft vector estimates for all values of $n = 1, \ldots, k$.

### *B. SCM with FDE*

We now consider the case in which SCM is used in conjunction with a CP and FDE; we refer to the discrete-time block-scheme reported in Fig. 2. A cyclic prefix of length $CM$ is added at the beginning of the block $\mathbf{s}$ of $L = kM$ QAM symbols, so as to have the vector $\widetilde{\mathbf{s}}$ of length $(k+C)M$. As in the previous case, the vector $\widetilde{\mathbf{s}}$ is passed through a serial-to-parallel conversion with $M$ outputs, a precoding block (again expressed through the matrix $\mathbf{Q}$), a bank of $N_T$ transmit filters; then conversion to RF and transmission take place. At the receiver, after baseband-conversion, the $N_R$ received signals are passed through a bank of filters matched to

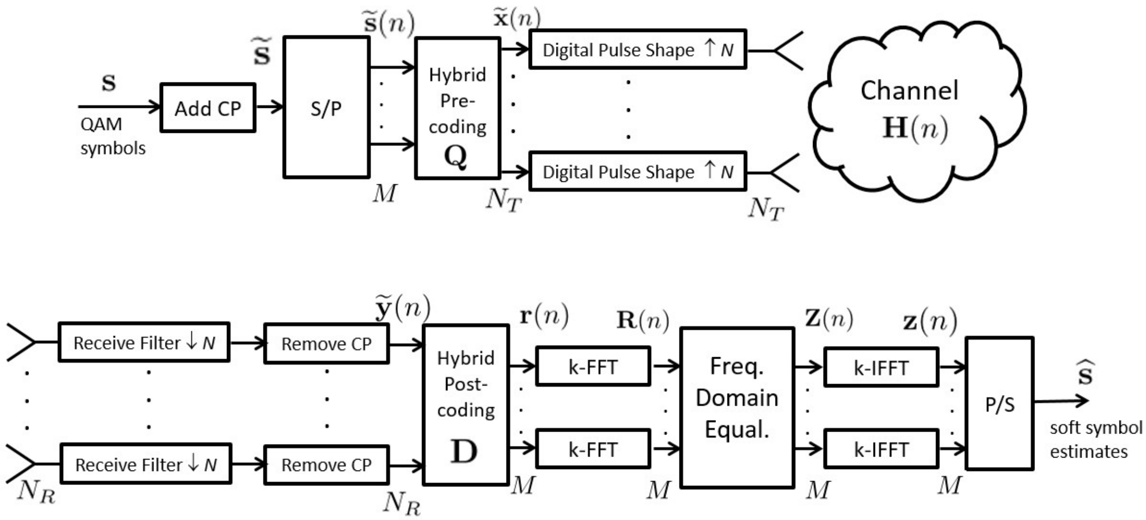


Figure 2. Transceiver block-scheme for SCM with cyclic prefix, FFT-based processing and FDE.

the ones used for transmission and sampled at symbol-rate; then, the cyclic prefix is removed. We thus obtain the $N_R$-dimensional vectors $\widetilde{\mathbf{y}}(n)$, with $n = 1, \ldots, k$, containing a noisy version of the *circular* convolution between the sequence $\widetilde{\mathbf{x}}(n)$ and $\widetilde{\mathbf{H}}(n)$ , i.e.:

$$\widetilde{\mathbf{y}}(n) = \widetilde{\mathbf{H}}(n) \circledast \widetilde{\mathbf{x}}(n) + \mathbf{w}(n) \ , \qquad n = 1, \ldots, k \tag{14}$$

The vectors $\widetilde{\mathbf{y}}(n)$ are then processed by the post-coding matrix $\mathbf{D}$. The choice of the matrices $\mathbf{Q}$ and $\mathbf{D}$ is the same as that of the previous subsection (SCM with TDE), so we do not comment on it here. After post-coding beamforming, we obtain the $M$-dimensional vectors $\mathbf{r}(n) = \mathbf{D}^H \widetilde{\mathbf{y}}(n)$, with $n = 1, \ldots, k$. These vectors go through an entry-wise FFT transformation on $k$ points; the $n$-th FFT coefficient, with $n = 1, \ldots, k$, can be shown to be expressed as

$$\mathbf{R}(n) = \widetilde{\mathcal{H}}(n)\mathbf{X}(n) + \mathbf{W}(n) \ , \tag{15}$$

where $\widetilde{\mathcal{H}}(n)$ is an $(M \times N_T)$-dimensional matrix representing the $n$-th FFT coefficient of the matrix-valued sequence $\mathbf{D}^H \widetilde{\mathbf{H}}(n)$, and $\mathbf{X}(n)$ and $\mathbf{W}(n)$ are the $n$-th FFT coefficient of the sequences $\widetilde{\mathbf{x}}(n)$ and $\mathbf{D}^H \mathbf{w}(n)$, respectively. From (15), it is seen that, due to the presence of multiple antennas, and, thus, of the matrix-valued channel, the useful symbols reciprocally interfere and an equalizer is needed. (15) can be also shown to be expressed as:

$$\mathbf{R}(n) = \widetilde{\mathcal{H}}(n)\mathbf{Q}\widetilde{\mathbf{S}}(n) + \mathbf{W}(n) \ , \tag{16}$$

with $\widetilde{\mathbf{S}}(n)$ an $M$-dimensional vector representing the $n$-th FFT coefficient of the vector-valued sequence $\widetilde{\mathbf{s}}(n)$.[2] We denote by $\mathbf{E}(n)$ the $(M \times M)$-dimensional equalization matrix, and a zero-forcing approach is adopted, thus implying that $\mathbf{E}^H(n) = (\widetilde{\mathcal{H}}(n)\mathbf{Q})^{-1}$. The output of the equalizer is written as

$$\mathbf{Z}(n) = \mathbf{E}^H(n)\mathbf{R}(n) = \widetilde{\mathbf{S}}(n) + (\widetilde{\mathcal{H}}(n)\mathbf{Q})^{-1}\mathbf{W}(n) \; .$$

Then, the vectors $\mathbf{Z}(n)$ go through an entry-wise IFFT transformation on $k$ points. It can be shown that the $n$-th IFFT coefficient of the vector $\mathbf{Z}(n)$ can be expressed as:

$$\mathbf{z}(n) = \widetilde{\mathbf{s}}(n) + \left[\mathbf{I}_M \otimes [\mathbf{D}_{\text{IFFT}}]_{:,n}\right] \mathbf{N}_{\text{stacked}} \; , \tag{17}$$

where $[\mathbf{D}_{\text{IFFT}}]_{:,n}$ is the $n$-th column of the isometric IFFT matrix $\mathbf{D}_{\text{IFFT}}$, whose $(m,l)$-th element is given by

$$\mathbf{D}_{\text{IFFT}}(m,l) = \frac{1}{\sqrt{k}} e^{j2\pi\frac{(m-1)(l-1)}{k}} \; ,$$

and $\mathbf{N}_{\text{stacked}}$ is the $kM$-dimensional vector containing the stacked vectors $(\widetilde{\mathcal{H}}(1)\mathbf{Q})^{-1}\mathbf{W}(1), \ldots, (\widetilde{\mathcal{H}}(k)\mathbf{Q})^{-1}\mathbf{W}(k)$.

*Considerations on complexity.* Looking at the scheme in Fig. 2, the computational burden of the considered transceiver architecture is the following. $2M$ FFTs of length $k$ are required, with a complexity proportional to $2Mk\log_2 k$; in order to compute the zero-forcing matrix, the FFT of the matrix-valued sequence $\widetilde{\mathcal{H}}(n)$ must be computed, with a complexity proportional to $MN_T(k\log_2 k)$; computation of the matrix $(\widetilde{\mathcal{H}}(n)\mathbf{Q})$ and of its inverse, for $n = 1, \ldots, k$, finally requires a computational burden proportional to $k(N_T M^2 + M^3)$.

It can be easily seen that the complexity of the FDE scheme is lower than that of the TDE scheme.

### *C. Transceiver model - OFDM*

Finally, we consider, for benchmarking purposes, the MIMO-OFDM discrete-time block-scheme reported in Fig. 3. Differently from previous schemes, we have explicitly separated the baseband digital beamforming from its analog counterparts; such a separation is needed in order to keep down system complexity, and to explicitly point out that while baseband FD

[2] We used here the relation $\mathbf{X}(n) = \mathbf{Q}\widetilde{\mathbf{S}}(n)$.

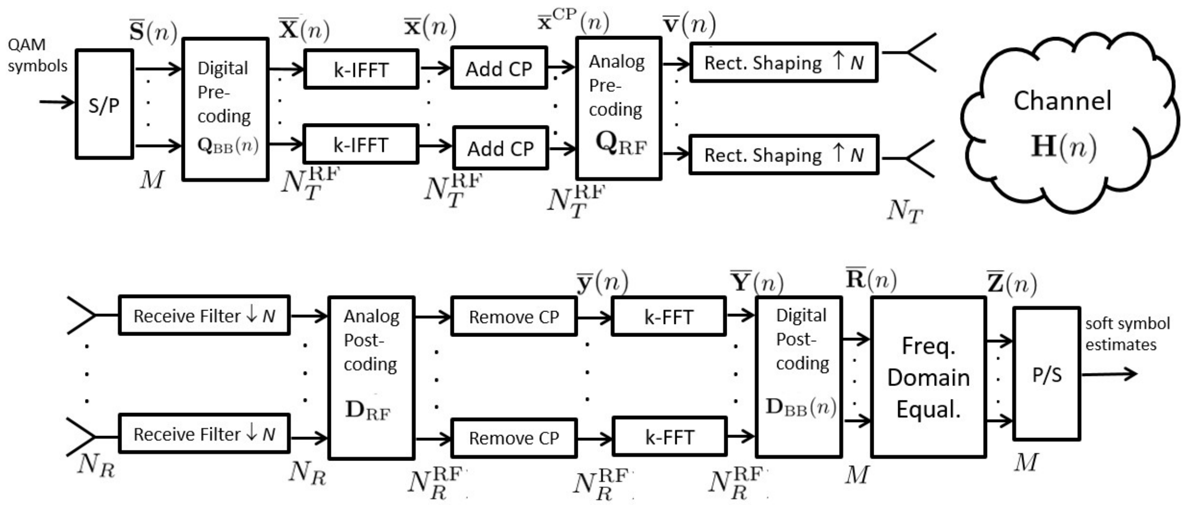


Figure 3. Transceiver block-scheme for OFDM with FDE.

beamforming is made on a "per-subcarrier" basis, the analog beamformer jointly process the entire signal bandwidth, i.e., all the subcarriers are treated uniformly. In Fig. 3, $N_T^{\mathrm{RF}}$ and $N_R^{\mathrm{RF}}$ RF chains are considered at the transmitter and at the receiver, and we have $M \leq N_T^{\mathrm{RF}} \leq N_T$ and $M \leq N_R^{\mathrm{RF}} \leq N_R$. Notice also that the choice $N_T^{\mathrm{RF}} = N_T$ and $N_R^{\mathrm{RF}} = N_R$ results in a non-hybrid, FD beamforming.

Each OFDM symbol is assumed to be made of $L = kM$ QAM data symbols; after S/P conversion, the data symbols are split in $k$ distinct $M$-dimensional vectors $\overline{\mathbf{S}}(1), \ldots, \overline{\mathbf{S}}(k)$. These vectors are pre-coded through the $(N_T^{\mathrm{RF}} \times M)$-dimensional digital precoding matrices $\mathbf{Q}_{\mathrm{BB}}(1), \ldots, \mathbf{Q}_{\mathrm{BB}}(n)$, thus yielding the vectors $\overline{\mathbf{X}}(n) = \mathbf{Q}_{\mathrm{BB}}(n)\overline{\mathbf{S}}(n)$ – note that we are here assuming that the digital pre-coding matrix is not constant over all the sub-carriers [19]. These vectors then go through an entry-wise IFFT transformation on $k$ points; we denote by $\overline{\mathbf{x}}(n)$ the $M$-dimensional transformed vectors, with $n = 1, \ldots, k$. A CP of length $C$ is added at the beginning of the block so that we have the following sequence of $N_T$-dimensional vectors:

$$\overline{\mathbf{x}}^{\mathrm{CP}}(n) = \begin{cases} \overline{\mathbf{x}}(n + k - C) \;, n = 1, \ldots, C \;, \\ \overline{\mathbf{x}}(n - C) \;, \qquad n = C + 1, \ldots, C + k \;. \end{cases} \tag{18}$$

The vectors $\overline{\mathbf{x}}^{\mathrm{CP}}(n)$ are precoded through the $(N_T \times N_T^{\mathrm{RF}})$-dimensional analog precoding matrix $\mathbf{Q}_{\mathrm{RF}}$, thus yielding the vectors $\overline{\mathbf{v}}(n) = \mathbf{Q}_{\mathrm{RF}}\overline{\mathbf{x}}^{\mathrm{CP}}(n)$. The vectors $\overline{\mathbf{v}}(n)$ are passed through a bank of $N_T$ transmit filters, converted to RF and transmitted. At the receiver, after baseband-conversion, the $N_R$ received signals are passed through a bank of filters matched to the ones used for transmission and sampled at symbol-rate; then, they are post-coded through the $(N_R \times N_R^{\mathrm{RF}})$-dimensional analog precoding matrix $\mathbf{D}_{\mathrm{RF}}$ and the cyclic prefix is removed. We thus obtain the following $N_R^{\mathrm{RF}}$-dimensional vectors $\overline{\mathbf{y}}(n)$, with $n = 1, \ldots, k$:

$$\overline{\mathbf{y}}(n) = \mathbf{D}_{\mathrm{RF}}^H \left[ \widetilde{\mathbf{H}}(n) \circledast \mathbf{Q}_{\mathrm{RF}} \overline{\mathbf{x}}(n) \right] + \mathbf{D}_{\mathrm{RF}}^H \mathbf{w}(n) \ , \tag{19}$$

with $\widetilde{\mathbf{H}}(n)$ denoting again the matrix-valued FIR filter representing the composite channel impulse response (i.e., the convolution of the transmit filter, actual matrix-valued channel and receive filter). These vectors go through an entry-wise FFT transformation on $k$ points; the $n$-th FFT coefficient, with $n = 1, \ldots, k$, can be shown to be expressed as

$$\overline{\mathbf{Y}}(n) = \mathbf{D}_{\mathrm{RF}}^H \overline{\mathcal{H}}(n) \mathbf{Q}_{\mathrm{RF}} \mathbf{Q}_{\mathrm{BB}}(n) \overline{\mathbf{S}}(n) + \mathbf{D}_{\mathrm{RF}}^H \overline{\mathbf{W}}(n) \ , \tag{20}$$

where $\overline{\mathcal{H}}(n)$ is an $(N_R \times N_T)$-dimensional matrix representing the $n$-th FFT coefficient of the matrix-valued sequence $\widetilde{\mathbf{H}}(n)$, and $\overline{\mathbf{W}}(n)$ is the $n$-th FFT coefficient of the sequence $\mathbf{w}(n)$, respectively. The vectors $\overline{\mathbf{Y}}(n)$ are then processed by the digital post-coding matrix $\mathbf{D}_{\mathrm{BB}}(n)$; we thus obtain the $M$-dimensional vectors

$$\overline{\mathbf{R}}(n) = \mathbf{D}_{\mathrm{BB}}^H(n) \mathbf{D}_{\mathrm{RF}}^H \overline{\mathcal{H}}(n) \mathbf{Q}_{\mathrm{RF}} \mathbf{Q}_{\mathrm{BB}}(n) \overline{\mathbf{S}}(n) + \mathbf{D}_{\mathrm{BB}}^H(n) \mathbf{D}_{\mathrm{RF}}^H \overline{\mathbf{W}}(n) \ , \quad n = 1, \ldots, k \ . \tag{21}$$

From (20), it is seen that, due to the presence of multiple antennas, and, thus, of the matrix-valued channel, the useful symbols reciprocally interfere and thus an equalizer is needed. Denoting by $\overline{\mathbf{E}}(n)$ the $(M \times M)$-dimensional equalization matrix, and using a zero-forcing approach, it can be seen that $\overline{\mathbf{E}}^H(n) = (\mathbf{D}_{\mathrm{BB}}^H(n) \mathbf{D}_{\mathrm{RF}} \overline{\mathcal{H}}(n) \mathbf{Q}_{\mathrm{RF}} \mathbf{Q}_{\mathrm{BB}}(n))^+$, where $(\cdot)^+$ denotes the Moore-Penrose pseudoinverse. The output of the equalizer can be shown to be expressed as:

$$\overline{\mathbf{Z}}(n) \ = \ \overline{\mathbf{E}}(n)^H \overline{\mathbf{R}}(n) \ = \ \overline{\mathbf{S}}(n) + (\mathbf{D}_{\mathrm{BB}}(n)^H \mathbf{D}_{\mathrm{RF}}^H \overline{\mathcal{H}}(n) \mathbf{Q}_{\mathrm{RF}} \mathbf{Q}_{\mathrm{BB}}(n))^+ \mathbf{D}_{\mathrm{BB}}(n)^H \mathbf{W}(n) \ . \tag{22}$$

After P/S conversion we finally obtain the soft estimates of the transmitted symbols.

## IV. Hybrid architecture design

We now detail the low-complexity hybrid beamforming structures. We first deal with the case of SCM, and then will examine the MIMO-OFDM case.

### A. Hybrid beamforming for SCM schemes

In order to reduce hardware complexity with respect to the FD beamforming, in hybrid structures the $(N_T \times M)-$dimensional pre-coding matrix is written as $\mathbf{Q} = \mathbf{Q}_{\rm RF}\mathbf{Q}_{\rm BB}$, where $\mathbf{Q}_{\rm RF}$ is the $(N_T \times N_T^{RF})$-dimensional RF precoding matrix and $\mathbf{Q}_{\rm BB}$ is the $(N_T^{RF} \times M)-$dimensional baseband precoding matrix. Since the RF precoder is implemented using phase shifters, the entries of the matrix $\mathbf{Q}_{RF}$ have all the same magnitude (equal to $\frac{1}{\sqrt{N_T}}$), and just differ for the phase. Now, denoting by $\mathbf{Q}^{\rm opt}$ the $(N_T \times M)-$dimensional FD beamforming that we would use in the situation of no hardware complexity constraints, the matrices $\mathbf{Q}_{\rm RF}$ and $\mathbf{Q}_{\rm BB}$ can be found by using the Frobenius norm as a distance metric and solving the following optimization problem:

$$\begin{aligned}(\mathbf{Q}_{\rm RF}^*, \mathbf{Q}_{\rm BB}^*) = & \arg\min_{\mathbf{Q}_{\rm RF}, \mathbf{Q}_{\rm BB}} ||\mathbf{Q}^{\rm opt} - \mathbf{Q}_{\rm RF}\mathbf{Q}_{\rm BB}||_F \\ \text{subject to} \qquad & |\mathbf{Q}_{\rm RF}(i,j)| = \frac{1}{\sqrt{N_T}} \ , \quad \forall i,j \\ & ||\mathbf{Q}_{\rm RF}\mathbf{Q}_{\rm BB}||_F^2 \leq M \ .\end{aligned} \tag{23}$$

Similarly, with regard to the design of the post-coding beamforming matrix, the optimal FD beamformer $\mathbf{D}^{\rm opt}$ that we would use in case of no hardware complexity constraints is approximated by the product $\mathbf{D}_{\rm RF}\mathbf{D}_{\rm BB}$, where $\mathbf{D}_{\rm RF}$ is the $(N_R \times N_R^{RF})-$dimensional RF post-coding matrix and $\mathbf{D}_{\rm BB}$ is the $(N_R^{RF} \times M)-$dimensional baseband post-coding matrix. The entries of the RF post-coder $\mathbf{D}_{\rm RF}$ are constrained to have norm equal to $\frac{1}{\sqrt{N_R}}$. The matrices $\mathbf{D}_{\rm RF}$ and $\mathbf{D}_{\rm BB}$ can be then found solving the following optimization problem

$$\begin{aligned}(\mathbf{D}_{\rm RF}^*, \mathbf{D}_{\rm BB}^*) = & \arg\min_{\mathbf{D}_{\rm RF}, \mathbf{D}_{\rm BB}} ||\mathbf{D}^{\rm opt} - \mathbf{D}_{\rm RF}\mathbf{D}_{\rm BB}||_F \\ \text{subject to} \qquad & |\mathbf{D}_{\rm RF}(i,j)| = \frac{1}{\sqrt{N_R}} \ , \quad \forall i,j \ .\end{aligned} \tag{24}$$

It is easy to show that optimization problems (23) and (24) are not convex optimization problem; inspired by [20], we thus resort to the Block Coordinate Descent for Subspace Decomposition (BCD-SD) algorithm, that basically is based on a sequential iterative update of the analog part and of the baseband part of the beamformers. The algorithm's recipe is reported in Algorithm 1.

**Algorithm 1** Block Coordinate Descent for Subspace Decomposition Algorithm for Hybrid Beamforming

1: Initialize $I_{\max}$ and set $i = 0$

2: Set arbitrary $\mathbf{Q}_{\mathrm{RF},0}$ and $\mathbf{D}_{\mathrm{RF},0}$

3: **repeat**

4: Update $\mathbf{Q}_{\mathrm{BB,i+1}} = \left(\mathbf{Q}^H_{\mathrm{RF,i}}\mathbf{Q}_{\mathrm{RF,i}}\right)^{-1}\mathbf{Q}^H_{\mathrm{RF,i}}\mathbf{Q}^{\mathrm{opt}}$
and $\mathbf{D}_{\mathrm{BB,i+1}} = \left(\mathbf{D}^H_{\mathrm{RF,i}}\mathbf{D}_{\mathrm{RF,i}}\right)^{-1}\mathbf{D}^H_{\mathrm{RF,i}}\mathbf{D}^{\mathrm{opt}}$

5: Set $\phi_i = \mathbf{Q}^{\mathrm{opt}}\mathbf{Q}^H_{\mathrm{BB,i+1}}\left(\mathbf{Q}_{\mathrm{BB,i+1}}\mathbf{Q}^H_{\mathrm{BB,i+1}}\right)^{-1}$
and $\psi_i = \mathbf{D}^{\mathrm{opt}}\mathbf{D}^H_{\mathrm{BB,i+1}}\left(\mathbf{D}_{\mathrm{BB,i+1}}\mathbf{D}^H_{\mathrm{BB,i+1}}\right)^{-1}$

6: Update $\mathbf{Q}_{\mathrm{RF,i}} = \frac{1}{\sqrt{N_T}}e^{j\phi_i}$
and $\mathbf{D}_{\mathrm{RF,i}} = \frac{1}{\sqrt{N_R}}e^{j\psi_i}$

7: Set $i = i + 1$

8: **until** convergence or $i = I_{\max}$

### *B. Hybrid beamforming for the MIMO-OFDM transceiver*

We now consider the issue of beamformer design for the MIMO-OFDM transceiver. From (21) it is seen that the optimal pre-coders and post-coders for the detection of the data vector $\overline{\mathbf{S}}(n)$ are given by the left and right singular vectors associated to the $M$ largest eigenvalues of the matrix $\overline{\mathcal{H}}(n)$, respectively. We will denote these optimal beamformers as $\mathbf{Q}^{\mathrm{opt}}(n)$ and $\mathbf{D}^{\mathrm{opt}}(n)$, respectively; differently from what happens for the SCM transceivers, these beamformers are now carrier dependent. Our aim is to approximate the optimal pre-coder $\mathbf{Q}^{\mathrm{opt}}(n)$ with the product $\mathbf{Q}_{\mathrm{RF}}\mathbf{Q}_{\mathrm{BB}}(n)$, and the optimal post-coder $\mathbf{D}^{\mathrm{opt}}(n)$ with the product $\mathbf{D}_{\mathrm{RF}}\mathbf{D}_{\mathrm{BB}}(n)$. Now, letting [19]:

$$\begin{aligned}
\mathbf{Q}^{\mathrm{opt}} &= [\mathbf{Q}^{\mathrm{opt}}(1), \ldots, \mathbf{Q}^{\mathrm{opt}}(k)] \quad \in \mathbb{C}^{N_T \times kM}\ , \\
\mathbf{D}^{\mathrm{opt}} &= [\mathbf{D}^{\mathrm{opt}}(1), \ldots, \mathbf{D}^{\mathrm{opt}}(k)] \quad \in \mathbb{C}^{N_R \times kM}\ , \\
\mathbf{Q}_{\mathrm{BB}} &= [\mathbf{Q}_{\mathrm{BB}}(1), \ldots, \mathbf{Q}_{\mathrm{BB}}(k)] \quad \in \mathbb{C}^{N_T^{RF} \times kM}\ , \\
\mathbf{D}_{\mathrm{BB}} &= [\mathbf{D}_{\mathrm{BB}}(1), \ldots, \mathbf{D}_{\mathrm{BB}}(k)] \quad \in \mathbb{C}^{N_R^{RF} \times kM}\ ,
\end{aligned}$$

the hybrid beamformer design amount to solving the following two constrained optimization problems

$$\begin{aligned} (\mathbf{Q}_{\mathrm{RF}}^{*}, \mathbf{Q}_{\mathrm{BB}}^{*}) = & \arg\min_{\mathbf{Q}_{\mathrm{RF}}, \mathbf{Q}_{\mathrm{BB}}} ||\mathbf{Q}^{\mathrm{opt}} - \mathbf{Q}_{\mathrm{RF}}\mathbf{Q}_{\mathrm{BB}}||_F \\ \text{subject to} \quad & |\mathbf{Q}_{\mathrm{RF}}(i,j)| = \tfrac{1}{\sqrt{N_T}} \ , \\ & \|\mathbf{Q}_{\mathrm{RF}}\mathbf{Q}_{\mathrm{BB,k}}\|_F^2 \le kM \ , \end{aligned} \tag{25}$$

and

$$\begin{aligned} (\mathbf{D}_{\mathrm{RF}}^{*}, \mathbf{D}_{\mathrm{BB}}^{*}) = & \arg\min_{\mathbf{D}_{\mathrm{RF}}, \mathbf{D}_{\mathrm{BB}}} ||\mathbf{D}^{\mathrm{opt}} - \mathbf{D}_{\mathrm{RF}}\mathbf{D}_{\mathrm{BB}}||_F \\ \text{subject to} \quad & |\mathbf{D}_{\mathrm{RF}}(i,j) = \tfrac{1}{\sqrt{N_R}} \ . \end{aligned} \tag{26}$$

The above optimization problems have the same structure as problems in (23) and (24), and can thus be solved through a straightforward application of the BCD-SD algorithm. We do not explicitly report here the full details of the algorithm for the sake of brevity.

## V. Computation of the achievable spectral efficiency

As a figure of merit to compare the different transceiver architectures we will use the ASE, that is the maximum achievable spectral efficiency with the constraint of arbitrarily small BER and of pre-fixed modulation type. The ASE takes the particular constellation and signaling parameters into consideration, so it does not qualify as a normalized capacity measure; (it is derived from the *constrained capacity*). We focus here on ergodic rates so the ASE is computed given the channel realization and averaged over it (remember that we are assuming perfect channel state information at the receiver). The spectral efficiency $\rho$ of any practical coded modulation system operating at a low packet error rate is upper bounded by the ASE, i.e., $\rho \le \mathrm{ASE}$, where

$$\mathrm{ASE} = \frac{1}{T_{\mathrm{s}}W} \lim_{L\to\infty} \frac{1}{L} E_{\widetilde{\mathbf{H}}}\left[ I(\mathbf{s};\hat{\mathbf{s}}|\widetilde{\mathbf{H}}) \right] \ \text{bit/s/Hz} \tag{27}$$

$I(\mathbf{s};\hat{\mathbf{s}}|\widetilde{\mathbf{H}})$ being the mutual information (given the channel realization) between the transmitted data symbols and their soft estimates, $T_{\mathrm{s}}$ the symbol interval, and $W$ the signal bandwidth (as specified in Section VI). Although not explicitly reported, for notational simplicity, the ASE in (27) depends on the Signal-to-Interference plus Noise Ratio (SINR).

The computation of the mutual information requires the knowledge of the channel conditional probability density function (pdf) $p(\hat{\mathbf{s}}|\mathbf{s},\widetilde{\mathbf{H}})$. As already said, it can be numerically computed by adopting the simulation-based technique described in [13] once the channel at hand is finite-memory and the optimal detector for it is available. In addition, only the optimal detector for the actual channel is able to achieve the ASE in (27).

In both transceiver models described in Section III the soft symbol estimates can be expressed in the form

$$\widehat{\mathbf{s}}(n) = \mathbf{C}\mathbf{s}(n) + \sum_{\ell \neq 0} \mathbf{C}_\ell \mathbf{s}(n-\ell) + \mathbf{z}(n) \tag{28}$$

i.e., as a linear transformation (through matrix $\mathbf{C}$, which eventually is zero in the FDE case with zero-forcing equalization) of the desired QAM data symbols, plus a linear combination of the interfering data symbols and the colored noise $\mathbf{z}(n)$ having a proper covariance matrix. The optimal receiver has a computational complexity which is out of reach and for this reason we consider much simpler linear suboptimal receivers. Hence, we are interested in the achievable performance when using suboptimal low-complexity detectors. We thus resort to the framework described in [13, Section VI]. We compute proper lower bounds on the mutual information (and thus on the ASE) obtained by substituting $p(\hat{\mathbf{s}}|\mathbf{s}, \tilde{\mathbf{H}})$ in the mutual information definition with an arbitrary auxiliary channel law $q(\hat{\mathbf{s}}|\mathbf{s}, \tilde{\mathbf{H}})$ with the same input and output alphabets as the original channel (mismatched detection [13])—the more accurately the auxiliary channel approximates the actual one, the closer the bound is. If the auxiliary channel law can be represented/described as a finite-state channel, the pdfs $q(\hat{\mathbf{s}}|\mathbf{s}, \tilde{\mathbf{H}})$ and $q_p(\hat{\mathbf{s}}|\tilde{\mathbf{H}}) = \sum_{\mathbf{s}} q(\hat{\mathbf{s}}|\mathbf{s}, \tilde{\mathbf{H}}) P(\mathbf{s})$ can be computed, this time, by using the optimal maximum a posteriori symbol detector for that auxiliary channel [13]. This detector, that is clearly suboptimal for the actual channel, has at its input the sequence $\hat{\mathbf{s}}$ generated by simulation *according to the actual channel model* (for details, see [13]). If we change the adopted receiver (or, equivalently, if we change the auxiliary channel) we obtain different lower bounds on the constrained capacity but, in any case, these bounds are *achievable* by those receivers, according to mismatched detection theory [13]. We thus say, with a slight abuse of terminology, that the computed lower bounds are the ASE values of the considered channel when those receivers are employed. This technique thus allows us to take reduced-complexity receivers into account. In fact, it is sufficient to consider an auxiliary channel which is a simplified version of the actual channel in the sense that only a portion of the actual channel memory and/or a limited number of impairments are present. In particular, we will use the auxiliary channel law (28), where the sum of the interference and the thermal noise $\mathbf{z}(n)$ is assimilated to Gaussian noise with a proper covariance matrix.

The transceiver models are compared in terms of ASE without taking into account specific coding schemes, being understood that, with a properly designed channel code, the information-theoretic performance can be closely approached.

## VI. Numerical Results

In our simulation setup, we consider a communication bandwidth of $W = 500$ MHz centered over a mmWave carrier frequency. The MIMO propagation channel, described in Section II, has been generated according to the statistical procedure detailed in [17]. The additive thermal noise is assumed to have a power spectral density of -174 dBm/Hz, while the front-end receiver is assumed to have a noise figure of 3 dB. We start by studying, in the following figures, the ASE for varying values of the transmit power $P_T$, of the distance $d$ between the transmitter and the receiver, of the number of transmit and receive antennas, of the multiplexing order $M$, and for the case in which the Root Raised Cosine (RRC) pulse with roll off factor 0.22 is adopted. For this waveform, we define the bandwidth as the frequency range such that out-of-band emissions are 40 dB below the maximum in-band value of the Fourier transform of the pulse. For the considered communication bandwidth of $W = 500$ MHz, we found that the symbol interval $T_\mathrm{s}$ is 1.98 ns, for the case in which we consider its truncated version to the interval $[-4T_\mathrm{s}, 4T_\mathrm{s}]$. The reported results are to be considered as an ideal benchmark for the ASE since we are neglecting the interference.[3] Hybrid pre-coding and post-coding, with $M$ RF chains at the transmitter and at the receiver, is considered, also in comparison to FD structures. Fig. 4 reports the ASE[4] of SCM-TDE, SCM-FDE and MIMO-OFDM using finite and infinite modulation cardinality versus the transmit power $P_T$ (varying in the range $[-50, 10]$ dBW), while instead in Fig. 5 the ASE for the three considered access schemes is reported versus the distance $d$ between the transmitter and the receiver, assuming that the transmit power is $P_T = 0$ dBW. While Fig. 4 contains a comparison between the 16-QAM modulation scheme and the case of Gaussian-distributed

[3]We note however that being mmWave systems mainly noise-limited rather than interference limited, the impact of this assumption on the obtained results is very limited.

[4]Of course, the achievable rates in bit/s can be immediately obtained by multiplying the ASE by the communication bandwidth $W = 500$ MHz.

data symbols, Fig. 5 focuses on the case of 4-QAM modulation and studies the impact of the multiplexing order $M$. Both these figures consider a link with $N_R \times N_T = 10 \times 50$.

We can see that the SCM-TDE performance is much better than the MIMO-OFDM and the SCM-FDE ones, with MIMO-OFDM slightly outperforming the SCM-FDE scheme. Figs. 6 focuses on the SCM-TDE scheme and reports the ASE versus the transmitted power $P_T$ (assuming a link length $d > 30$ m), studying the impact of the multiplexing order and of the size of the antenna arrays, while Fig. 7 reports, again for the SCM-TDE scheme, the ASE versus the link length (assuming $P_T = 0$ dBW), studying the impact of the modulation cardinality and of the size of the antenna arrays. Inspecting the figures, the following remarks are in order:

- Results, in general, as it is obvious, improve for increasing transmit power, for decreasing distance $d$ between transmitter and receiver and for increasing values of the number of transmit and receive antennas.
- In particular, a good performance can be attained for distances up to 100 m, whereas for $d > 100$ m we have a steep degradation of the ASE. In this region, all the advantages given by increasing the modulation cardinality or the number of antennas are essentially lost or reduced at very small values. Of course, this performance degradation may be compensated by increasing the transmit power.
- Regarding the multiplexing index $M$, it is interesting to note from Fig. 5 that for short distances the system benefits from a large multiplexing order, while, for large distances (which essentially correspond to low signal-to-noise ratio), the ASE corresponding to $M = 1$ is larger than that corresponding to the choice $M > 1$. This behavior is in agreement with the well-known result that for low signal-to-noise ratio there is no advantage in increasing the multiplexing order.
- For a reference distance of 30 m (which will be a typical one in small-cell 5G mmWave deployments for densely crowded areas), a transmit power around 0 dBW is enough to grant good performance and to benefit from the advantages of increased modulation cardinality, size of the antenna array, and multiplexing order.

We now proceed to showing BER results. In Figs 8, 9 and 10 we report the BER results respectively of 16QAM SCM-TDE, SCM-FDE and MIMO-OFDM when employing low-density-parity-check (LDPC) codes of rate equal to 1/2 and 9/10, in order to show how practical (i.e.,

Table I

CODE RATES AND DEGREE DISTRIBUTIONS OF THE EMPLOYED LDPC CODES.

| $r_c$ | variable node distribution | check node distribution |
|---|---|---|
| 1/2 | $a_2 = 0.499985$ $a_3 = 0.3$ $a_8 = 0.200015$ | $a_7 = 0.999815$ $a_8 = 0.000185185$ |
| 9/10 | $a_2 = 0.0999846$ $a_3 = 0.8$ $a_4 = 0.1111111$ | $a_{30} = 0.999691$ $a_{31} = 0.000308642$ |

finite-length and not *ad hoc* designed) codes perform in one realization of the considered scenario, which entails $M = 2$, $d = 30$ m, $N_R \times N_T = 10 \times 50$. The parameters of the codes are reported in Table I where $r_c$ denotes the rate of the code and the degree distributions of variable and check nodes are provided by giving the fraction $a_i$ ($\sum_i a_i = 1$) of degree $i$ nodes. In any case, the codeword length is $N = 64800$ bits, and the decoder iterations are limited to 40. These codes were designed for low intersymbol interference (ISI) channels, and, despite not specifically designed for these systems, they closely approach the provided ASE lower bounds. Since with $M = 2$ the two multiplexed streams perform differently, the code rates on each stream should be tailored accordingly.

## VII. CONCLUSION

This paper has provided a comparison between single-carrier modulation schemes and conventional OFDM for a MIMO link operating at mmWave frequencies. In particular, two SCM techniques have been considered, SCM-TDE and SCM-FDE, and these transceivers have been compared with the MIMO-OFDM scheme. Our analysis has taken into account both the peculiarity of the channel matrix at mmWave frequencies (a clustered model has been adopted), and the adoption of hybrid analog/digital beamforming structures. Results have shown that the SCM-TDE structure achieves superior performance with respect to the other two competing schemes, with the MIMO-OFDM slightly outperforming the SCM-FDE scheme. The present study can be generalized and strengthened in many directions. First of all, the considered analysis might be applied in a multiuser environment; then, since, as already discussed, the reduced wavelength of mmWave frequencies permits installing arrays with many antennas in small volumes, an analysis, possibly through asymptotic analytic considerations, of the very large number of antennas regime could also be made. Last, but not least, energy-efficiency considerations should also be made: both the ASE and the transceiver power consumption increase for increasing transmit power and increasing size of the antenna arrays; if we focus on the ratio between the ASE and the transceiver power consumption, namely on the system energy efficiency, optimal trade-off values for the transmit power and size of the antenna arrays should be found. These topics are certainly worth future investigation.

## REFERENCES


[1] J. G. Andrews, S. Buzzi, W. Choi, S. Hanly, A. Lozano, A. C. Soong, and J. C. Zhang, "What will 5G be?" *IEEE J. Select. Areas Commun.*, vol. 32, no. 6, Jun. 2014.

[2] A. Ghosh, T. A. Thomas, M. Cudak, R. Ratasuk, P. Moorut, F. W. Vook, T. Rappaport, J. G. R MacCartney, S. Sun, and S. Nie, "Millimeter wave enhanced local area systems: A high data rate approach for future wireless networks," *IEEE J. Select. Areas Commun.*, vol. 32, no. 6, pp. 1152 – 1163, Jun. 2014.

[3] T. S. Rappaport, S. Sun, R. Mayzus, H. Zhao, Y. Azar, K. Wang, G. N. Wong, J. K. Schulz, M. Samimi, and F. Gutierrez, "Millimeter wave mobile communications for 5G cellular: It will work!" *IEEE Access*, vol. 1, pp. 335–349, May 2013.

[4] T. S. Rappaport, F. Gutierrez, E. Ben-Dor, J. Murdock, Y. Qiao, and J. I. Tamir, "Broadband millimeter-wave propagation measurements and models using adaptive-beam antennas for outdoor urban cellular communications," *IEEE Trans. Antennas and Prop.*, vol. 61, no. 4, pp. 1850–1859, Apr. 2013.

[5] T. Bai, A. Alkhateeb, and R. Heath, "Coverage and capacity of millimeter-wave cellular networks," *IEEE Commun. Mag.*, vol. 52, no. 9, pp. 70–77, Sep. 2014.

[6] A. Alkhateeb, J. Mo, N. Gonzalez-Prelcic, and R. Heath, "MIMO precoding and combining solutions for millimeter-wave systems," *IEEE Commun. Mag.*, vol. 52, no. 12, pp. 122–131, Dec. 2014.

[7] V. Frascolla, M. Faerber, E. C. Strinati, L. Dussopt, V. Kotzsch, E. Ohlmer, M. Shariat, J. Putkonen, and G. Romano, "Mmwave use cases and prototyping: A way towards 5G standardization," in *Networks and Communications (EuCNC), 2015 European Conference on*, Jun. 2015, pp. 128–132.

[8] P. Banelli, S. Buzzi, G. Colavolpe, A. Modenini, F. Rusek, and A. Ugolini, "Modulation formats and waveforms for 5G networks: Who will be the heir of OFDM?" *IEEE Signal Processing Mag.*, vol. 31, no. 6, pp. 80–93, Nov. 2014.

[9] L. Deneire, B. Gyselinckx, and M. Engels, "Training sequence versus cyclic prefix-a new look on single carrier communication," *IEEE Communication Letters*, vol. 5, no. 7, pp. 292–294, Jul. 2001.

[10] M. Cudak *et al.*, "Moving towards mmwave-based beyond-4G (b-4G) technology," in *Proc. IEEE 77th VTC Spring*, Jun. 2013.

[11] S. Larew, T. Thomas, M. Cudak, and A. Ghosh, "Air interface design and ray tracing study for 5G millimeter wave communications," in *2013 IEEE Globecom Workshops*, Dec 2013, pp. 117–122.

[12] R. W. Heath, N. Gonzalez-Prelcic, S. Rangan, W. Roh, and A. Sayeed, "An overview of signal processing techniques for millimeter wave MIMO systems," *IEEE Journal of Selected Topics in Signal Processing*, vol. 10, no. 3, pp. 436–453, Feb. 2016.

[13] D. M. Arnold, H.-A. Loeliger, P. O. Vontobel, A. Kavčić, and W. Zeng, "Simulation-based computation of information rates for channels with memory," *IEEE Trans. Inform. Theory*, vol. 52, no. 8, pp. 3498–3508, Aug. 2006.

[14] A. Barbieri, D. Fertonani, and G. Colavolpe, "Time-frequency packing for linear modulations: spectral efficiency and practical detection schemes," *IEEE Transactions on Communications*, vol. 57, no. 10, pp. 2951–2959, Oct. 2009.

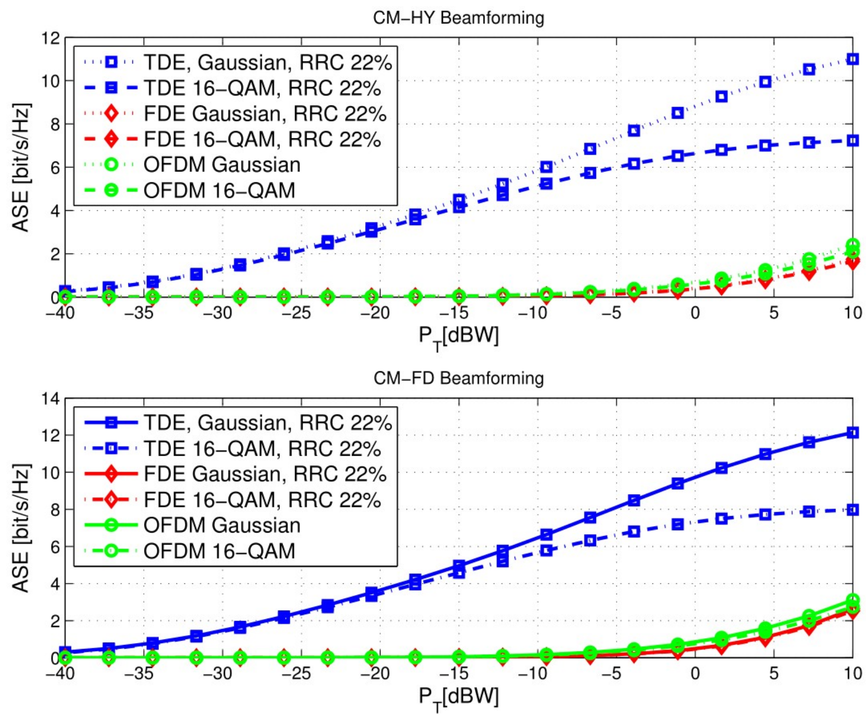


Figure 4. ASE versus transmit power; comparison of TDE, FDE and OFDM, with finite and infinite modulation cardinality and with comparison of hybrid (CM-HY) and digital (CM-FD) beamforming. Parameters: $M = 2$; $d = 30$ m $N_R \times N_T = 10 \times 50$.


[15] S. Buzzi, C. Risi, and G. Colavolpe, "Green and fast DSL via joint processing of multiple lines and time-frequency packed modulation," *Physical Communication*, vol. 13, Part C, pp. 99 – 108, Dec. 2014.

[16] O. El Ayach, S. Rajagopal, S. Abu-Surra, Z. Pi, and R. Heath, "Spatially sparse precoding in millimeter wave MIMO systems," *IEEE Trans. on Wireless Commun.*, vol. 13, no. 3, pp. 1499–1513, Mar. 2014.

[17] S. Buzzi and C. D'Andrea, "On clustered statistical MIMO millimeter wave channel simulation," *Arxiv e-prints [online] Available: http://arxiv.org/pdf/1604.00648v2.pdf*, May 2016.

[18] S. M. Kay, *Fundamentals of statistical signal processing, Volume 1: Estimation theory*. Prentice-Hall, 1998.

[19] M. Iwanow, N. Vucic, M. Castaneda, J. Luo, W. Xu, and W. Utschick, "Some aspects on hybrid wideband transceiver design for mmwave communication systems," *Proc. of 20th International ITG Workshop on Smart Antennas (WSA 2016)*, Jun. 2016.

[20] H. Ghauch, T. Kim, M. Bengtsson, and M. Skoglund, "Subspace estimation and decomposition for large millimeter-wave MIMO systems," *IEEE Journal of Selected Topics in Signal Processing*, vol. 10, no. 3, pp. 528–542, Apr. 2016.

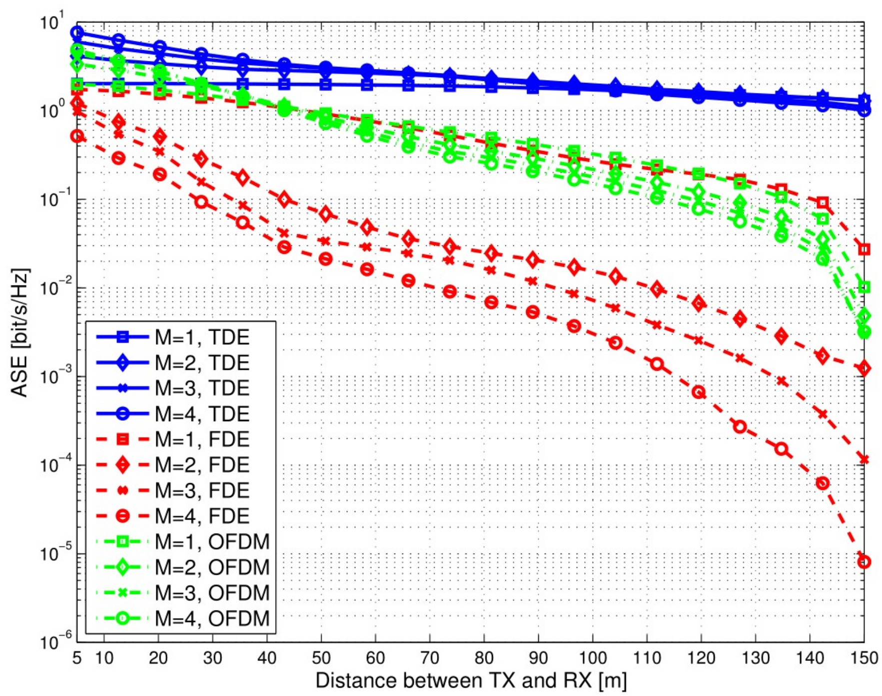


Figure 5. ASE versus distance; impact of multiplexing order, comparison of hybrid (CM-HY) and digital (CM-FD) beamforming with TDE, FDE and OFDM. Parameters: 4-QAM modulation; $P_T = 0$ dBW; $N_R \times N_T = 10 \times 50$.

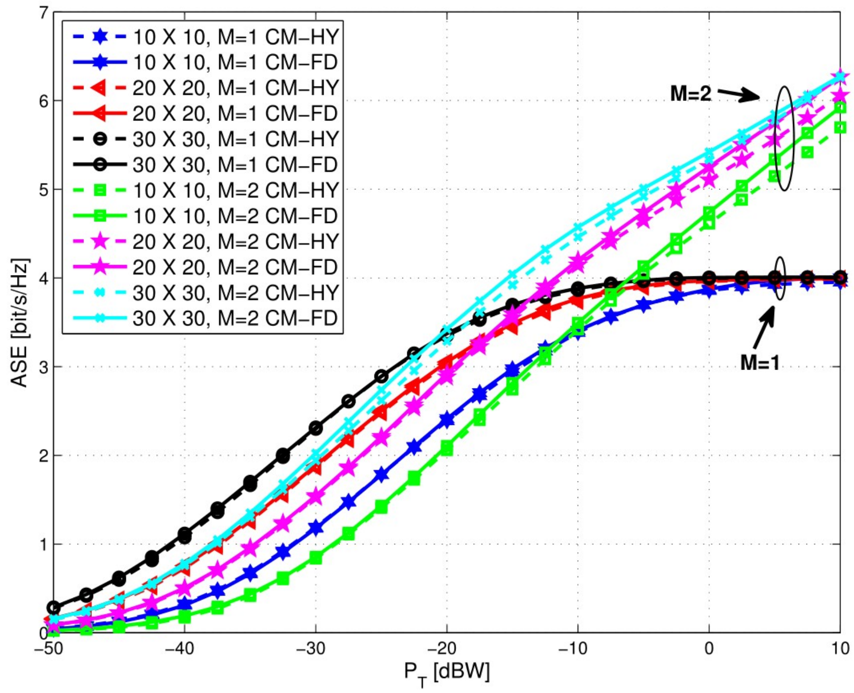


Figure 6. ASE versus transmit power; impact of array size, multiplexing order and comparison of hybrid (CM-HY) and digital (CM-FD) beamforming. Parameters: 16-QAM modulation; $d = 30$ m; varying $N_R \times N_T$.

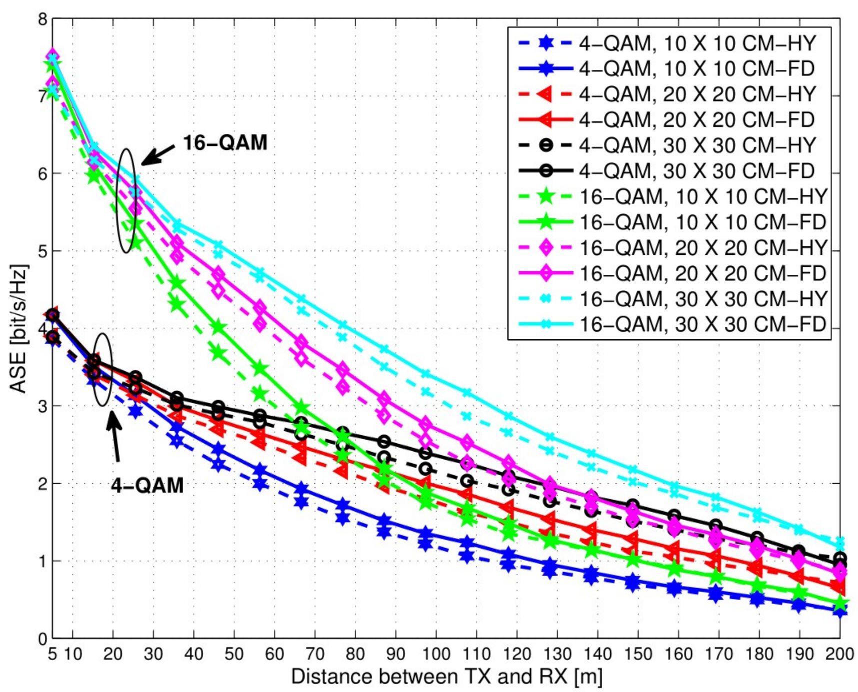


Figure 7. ASE versus distance; impact of modulation cardinality, array size and comparison of hybrid (CM-HY) and digital (CM-FD) beamforming. Parameters: $P_T = 0$ dBW; $M = 2$; varying $N_R \times N_T$.

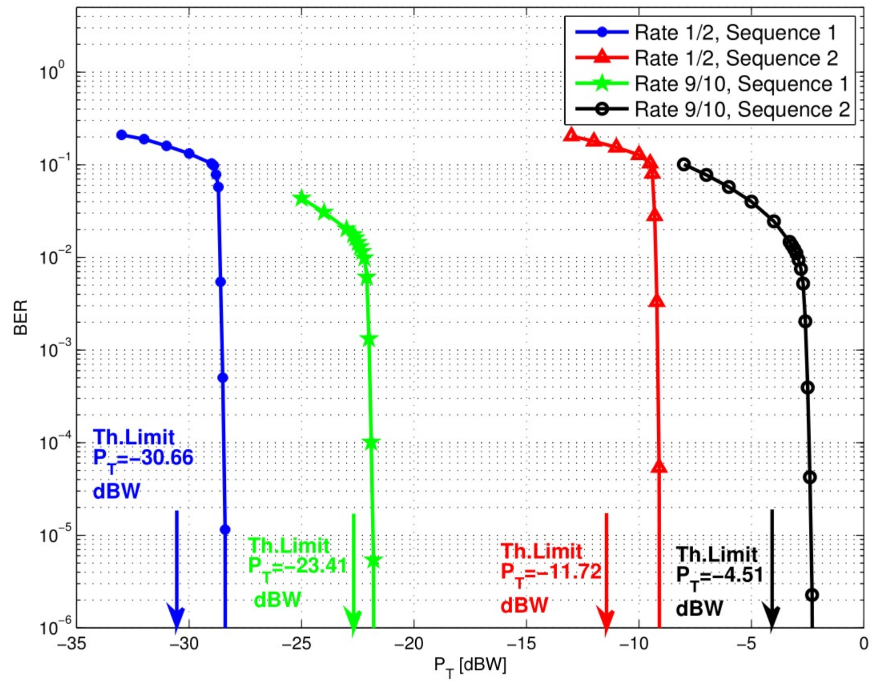


Figure 8. BER of TDE for 16QAM, d=30 m, $M$=2, $N_R \times N_T = 10 \times 50$.

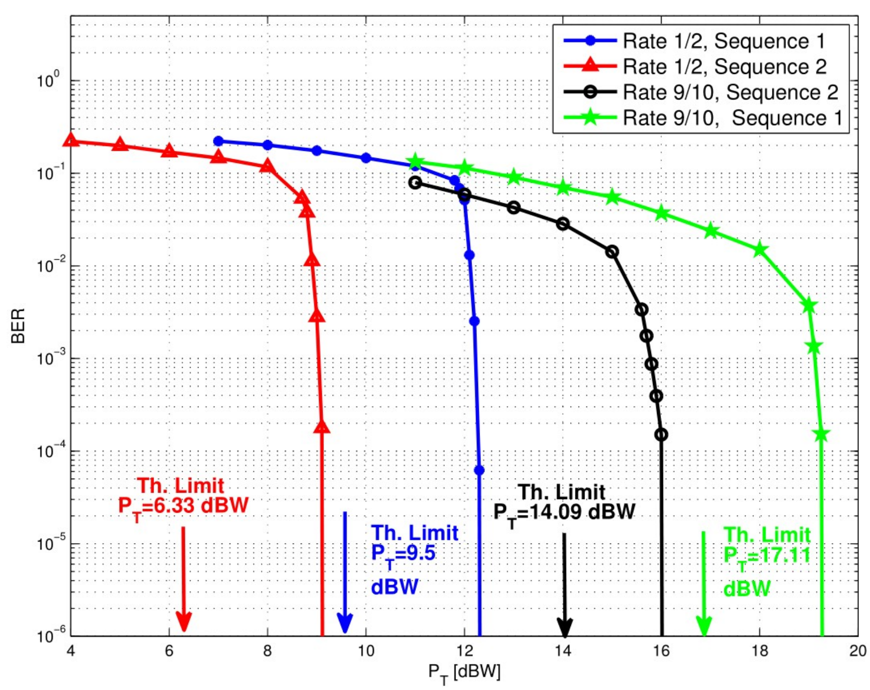


Figure 9. BER of FDE for 16QAM, d=30 m, $M$=2, $N_R \times N_T = 10 \times 50$.

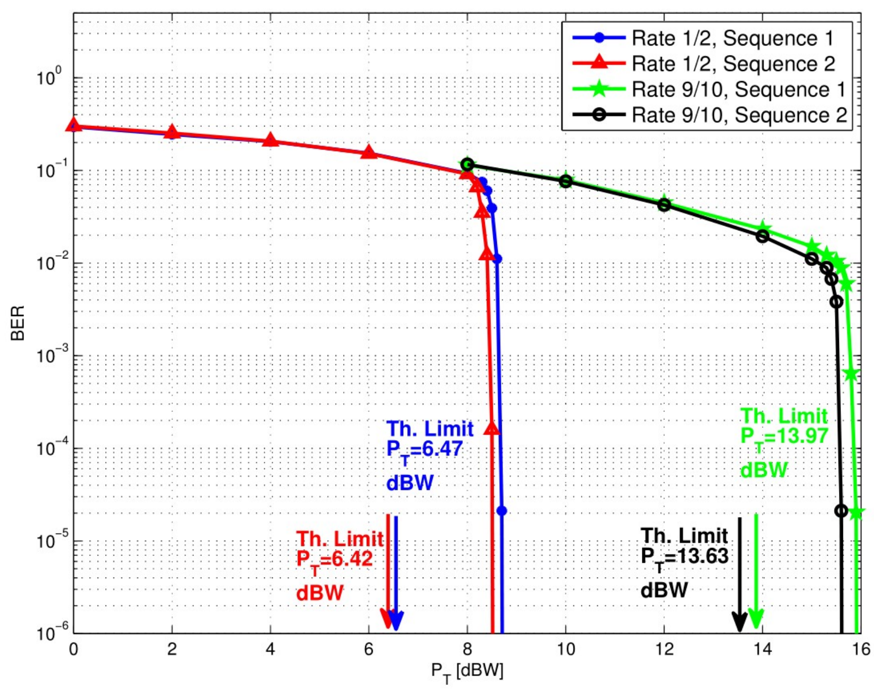


Figure 10. BER of OFDM for 16QAM, d=30 m, $M$=2, $N_R \times N_T = 10 \times 50$.

# Single-Carrier Modulation versus OFDM for Millimeter-Wave Wireless MIMO

Stefano Buzzi, *Senior Member, IEEE*, Carmen D'Andrea, Tommaso Foggi, Alessandro Ugolini, and Giulio Colavolpe, *Senior Member*

***Abstract*—Future wireless networks will extensively rely upon carrier frequencies larger than 10 GHz. Indeed, recent research has shown that, despite the large path-loss, millimeter wave (mmWave) frequencies can be successfully exploited to transmit very large data-rates over short distances to slowly moving users. This paper presents results on the achievable spectral efficiency on a wireless MIMO link operating at mmWave in a typical 5G scenario. Two different single-carrier modem schemes are considered, i.e., a traditional modulation scheme with linear equalization at the receiver, and a single-carrier modulation with cyclic prefix, frequency-domain equalization and FFT-based processing at the receiver; these two schemes are compared with a conventional MIMO-OFDM transceiver structure. Our analysis takes into account the peculiar characteristics of MIMO channels at mmWave frequencies, the use of hybrid (analog-digital) pre-coding and post-coding beamformers, and the finite cardinality of the modulation structure. Our results show that the best performance is achieved by single-carrier modulation with time-domain equalization, while MIMO-OFDM performs slightly better than single carrier modulation with frequency-domain equalization. Results also confirm that the spectral efficiency increases with the dimension of the antenna array, as well as that performance gets severely degraded when the link length exceeds 90-100 meters and the transmit power falls below 0 dBW.**

***Index Terms*—mmWave, 5G, MIMO, single-carrier modulation, spectral efficiency, MIMO-OFDM, time-domain equalization, frequency-domain equalization, hybrid decoding.**

## I. Introduction

The use of carrier frequencies larger than 10 GHz will be one of the main new features of fifth-generation (5G) wireless networks [1], and, due to the availability of large and currently unused bandwidths, will be instrumental in delivering gigabit data-rates per users. Until few years ago, the use of mmWave frequencies for cellular communications had been neglected due to the higher atmospheric absorption that they suffer compared to other frequency bands and to the larger values of the free-space path-loss. However, recent measurements suggest that mmWave attenuation is only slightly worse than in other bands, as far as propagation in dense urban environments and over short distances (up to about 100 meters) is concerned [2]. Additionally, since antennas at these wavelengths are very small, arrays with several elements can be packed in small volumes, in principle also on mobile devices, thus removing the traditional constraint that only few antennas can be placed on a smartphone and benefiting of an array gain at both edges of the communication link with respect to traditional cellular links. A large body of work has been recently carried out on the use of mmWave frequencies for cellular communications [2]–[6]. Nowadays, several prototypes and test-beds showing the potentiality of mmWave frequencies for cellular applications are already available [7] and the EU-funded project 5G-CHAMPION is planning a large scale demo for the 2018 Winter Olympic Games in Seoul (Republic of Korea) at 28 GHz frequency.

One of the key questions about the use of mmWave frequencies and in general about 5G cellular systems is about the type of modulation that will be used at these frequencies. Indeed, while it is not even sure that 5G systems will use orthogonal frequency division multiplexing (OFDM) modulation at classical cellular frequencies [8], there are reasons that push for 5G networks operating a single-carrier modulation (SCM) at mmWave frequencies [2]. First of all, the propagation attenuation of mmWave frequencies makes them a viable technology only for small-cell, dense networks, where few users will be associated to any given base station, thus implying that the efficient frequency-multiplexing features of OFDM may not be really needed. Additionally, the large bandwidth would cause low OFDM symbol duration, which, coupled with small propagation delays, means that the users may be multiplexed in the time domain as efficiently as in the frequency domain. Finally, mmWave frequencies will be operated together with massive antenna arrays to overcome propagation attenuation. This makes digital beamforming unfeasible, since the energy required for digital-to-analog and analog-to-digital conversion would be huge. Thus, each user will have an own radio-frequency beamforming, which requires users to be separated in time rather than frequency. For efficient removal of the intersymbol interference induced by the frequency-selective nature of the channel, the use of SCM coupled with a cyclic prefix has been proposed, so that FFT-based processing might be performed at the receiver [9]. In [10], [11], the null cyclic prefix single carrier (NCP-SC) scheme has been proposed for mmWave frequencies. The concept is to transmit a single-carrier signal, in which the usual cyclic prefix used by OFDM is replaced by nulls appended at the end of each transmit symbol. Given the cited prohibitive hardware complexity of fully-digital (FD) beamforming structures, several mmWave-specific MIMO architectures have been proposed, where signal processing is accomplished in a mixture of analog and digital

S. Buzzi and C. D'Andrea are with the Department of Electrical and Information Engineering, University of Cassino and Lazio Meridionale, I-03043 Cassino, Italy ({buzzi, carmen.dandrea}@unicas.it).

T. Foggi, A. Ugolini and G. Colavolpe are with the Department of Information Engineering, University of Parma, I-43100 Parma, Italy (tommaso.foggi@nemo.unipr.it, {alessandro.ugolini, giulio}@unipr.it).

This paper was partly presented at the 20th International ITG Workshop on Smart Antennas, Munich, Germany, March 2016.

domains (see, for instance, [12] and references therein). In particular, while FD beamforming requires one RF chain for each antenna, in hybrid structures a reduced number of RF chains is used, and beamforming is made partially in the digital domain and partially at RF frequencies, where only the signal phase (and not the amplitude) can be tuned prior to antenna trasmission.

This paper is concerned with the evaluation of the achievable spectral efficiency (ASE) of SCM schemes operating over MIMO links at mmWave frequencies. We consider three possible transceiver architectures: (a) SCM with linear minimum mean square error (LMMSE) equalization in the time domain for intersymbol interference removal and symbol-by-symbol detection; (b) SCM with cyclic prefix and FFT-based processing and LMMSE equalization in the frequency domain at the receiver; and (c) plain MIMO-OFDM architecture for benchmarking purposes. The ASE is computed by using the simulation-based technique for computing information-rates reported in [13]; this technique, that has been already used in several other cases [14], [15], permits taking into account the finite cardinality of the modulation, and thus provides more accurate results than the ones that are usually reported in the literature and that refer to Gaussian signaling. The considered transceiver structures use hybrid pre-coding and post-coding beamforming structures, with a number of RF chains equal to the used multiplexing order - this is indeed the minimum possible number of RF chains and so the resulting structures are the one with the lowest complexity. We also provide an analysis of the system bit-error-rate (BER), under the assumption that low-density parity-check (LDPC) codes are used. Our results will show that, among the three considered transceiver schemes, SCM with time-domain equalization (SCM-TDM) achieves by far the best performance, while MIMO-OFDM is only slightly better than SCM with frequency-domain equalization (SCM-FDE). Moreover, our results provide a further confirmation of the fact that for distances up to 100 meters, and with a transmit power around 0 dBW, mmWave links exhibit a very good performance and may be very useful in wireless cellular applications; for larger distances instead, either larger values of the transmit power or a larger number of antennas must be employed to overcome the distance-dependent increased attenuation.

The rest of this paper is organized as follows. Next Section contains the system model, with details on the considered mmWave channel model and on the front-end transmitter and receiver. In Section III the three considered transceiver structures, namely SCM-TDE, SCM-FDE and MIMO-OFDM, are accurately described, while the design of the hybrid precoding and post-coding beamforming structures is reported in Section IV. Extensive numerical results on the system ASE and on the coded BER are illustrated and discussed in Section V, while, finally, Section VI contains concluding remarks.

*Notation:* The symbol $(\cdot)^H$ denotes conjugate transpose, $(\cdot)^T$ denotes transpose, and $\mathbf{I}_N$ denotes the $(N \times N)$-dimensional identity matrix. The symbol $\circledast$ denotes circular convolution, $\mathrm{E}[\cdot]$ denotes expectation, while, finally, $\|\cdot\|_{\mathrm{F}}$ denotes the Frobenius norm.

## II. System model

We consider a transmitter-receiver pair that may be representative of either the uplink or the downlink of a cellular system. We denote by $N_T$ and $N_R$ the number of transmit and receive antennas, respectively, and consider the general case of a frequency-selective channel.

### A. The channel model

The propagation channel can be modeled as an $(N_R \times N_T)$-dimensional matrix-valued continuous time function, that we denote by $\mathbf{H}(t)$. According to the popular clustered model for MIMO mmWave channels, we assume that the propagation environment is made of $N_{\rm cl}$ scattering clusters, each of which contributes with $N_{{\rm ray},i}$ propagation paths $i = 1, \ldots, N_{\rm cl}$, plus a possibly present LOS component. We denote by $\phi^r_{i,l}$ and $\phi^t_{i,l}$ the azimuth angles of arrival and departure of the $l^{th}$ ray in the $i^{th}$ scattering cluster, respectively; similarly, $\theta^r_{i,l}$ and $\theta^t_{i,l}$ are the elevation angles of arrival and departure of the $l^{th}$ ray in the $i^{th}$ scattering cluster, respectively. Denoting by $h_{\rm TX}(t)$ the baseband equivalent transmit shaping filters,[1] by $h_{\rm RX}(t)$ the baseband equivalent of the impulse response of the $N_R$ receive filters, and by $h(t) = h_{\rm TX}(t) * h_{\rm RX}(t)$ their convolution, and assuming a sampling interval equal to $T_s$, the impulse-response of the linear time-invariant system consisting of the $N_T$ transmit shaping filters, the propagation channel, and the $N_R$ receive filters is a matrix-valued (of dimension $N_R \times N_T$) discrete-time sequence that can be written as follows:

$$
\begin{aligned}
\widetilde{\mathbf{H}}(n) = \gamma \sum_{i=1}^{N_{\rm cl}} \sum_{l=1}^{N_{{\rm ray},i}} \alpha_{i,l} \sqrt{L(r_{i,l})} \mathbf{a}_r(\phi^r_{i,l}, \theta^r_{i,l}) \cdot \\
\mathbf{a}_t^H(\phi^t_{i,l}, \theta^t_{i,l}) h(nT_s - \tau_{i,l}) + \widetilde{\mathbf{H}}_{\rm LOS}(n) \, . \quad (1)
\end{aligned}
$$

In the above equation, $\alpha_{i,l}$ and $L(r_{i,l})$ are the complex path gain and the attenuation associated to the $(i,l)$-th propagation path (whose length is denoted by $r_{i,l}$), respectively; $\tau_{i,l} = r_{i,l}/c$, with $c$ the speed of light, is the propagation delay associated with the $(i,l)$-th path. The complex gain $\alpha_{i,l} \sim \mathcal{CN}(0, \sigma^2_{\alpha,i})$, with $\sigma^2_{\alpha,i} = 1$ [16]. The factors $\mathbf{a}_r(\phi^r_{i,l}, \theta^r_{i,l})$ and $\mathbf{a}_t(\phi^t_{i,l}, \theta^t_{i,l})$ represent the normalized receive and transmit array response vectors evaluated at the corresponding angles of arrival and departure; additionally, $\gamma = \sqrt{\frac{N_R N_T}{\sum_{i=1}^{N_{\rm cl}} N_{{\rm ray},i}}}$ is a normalization factor ensuring that the received signal power scales linearly with the product $N_R N_T$. Regarding the array response vectors $\mathbf{a}_r(\phi^r_{i,l}, \theta^r_{i,l})$ and $\mathbf{a}_t(\phi^t_{i,l}, \theta^t_{i,l})$, a planar antenna array configuration is used for the transmitter and receiver, with $Y_r$, $Z_r$ and $Y_t$, $Z_t$ antennas respectively on the horizontal and vertical axes for the receiver and for the transmitter. Letting $k = 2\pi/\lambda$, $\lambda$ the considered wavelength, and denoting by $\tilde{d}$ the inter-element spacing we have

$$
\begin{aligned}
\mathbf{a}_x(\phi^x_{i,l}, \theta^x_{i,l}) = \tfrac{1}{\sqrt{Y_x Z_x}} [1, \ldots, e^{-jk\tilde{d}(m \sin\phi^x_{i,l} \sin\theta^x_{i,l} + n \cos\theta^x_{i,l})}, \\
\ldots, e^{-jk\tilde{d}((Y_x-1)\sin\phi^x_{i,l} \sin\theta^x_{i,l} + (Z_x-1)\cos\theta^x_{i,l})}] \, ,
\end{aligned}
$$

where $x$ may be either $r$ or $t$. Let us now comment on the LOS component $\widetilde{\mathbf{H}}_{\rm LOS}(n)$ in (1). Denoting by $\phi^r_{\rm LOS}$, $\phi^t_{\rm LOS}$, $\theta^r_{\rm LOS}$,

[1] We have $N_T$ of such filters.

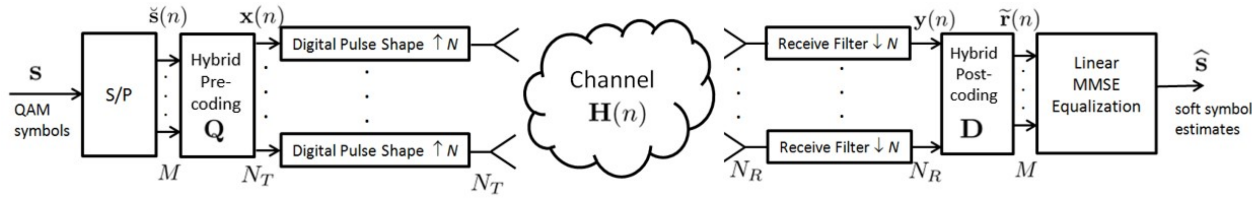


Figure 1. Transceiver block-scheme for SCM with TDE.

and $\theta^t_{\rm LOS}$ the departure angles corresponding to the LOS link, we assume that

$$\mathbf{H}_{\rm LOS}(n) = I_{\rm LOS}(d)\sqrt{N_R N_T}e^{j\eta}\sqrt{L(d)}\mathbf{a}_r(\phi^r_{\rm LOS},\theta^r_{\rm LOS})\cdot \mathbf{a}_t^H(\phi^t_{\rm LOS},\theta^t_{\rm LOS})h(nT_s-\tau_{\rm LOS}) \; . \tag{2}$$

In the above equation, $\eta \sim \mathcal{U}(0,2\pi)$, while $I_{\rm LOS}(d)$ is an indicator function/Bernoulli random variable, equal to 1 if a LOS link exists between transmitter and receiver. We refer the reader to [17] for a complete specification of all the channel parameters needed to describe the channel model in (1). Assuming that the multipath delay spread spans $P$ sampling intervals and that the duration of the transmit and receive shaping filters spans $P_h$ sampling intervals each, it is easily seen that the matrix-valued channel sequence $\widetilde{\mathbf{H}}(n)$ has $\widetilde{P} = P + 2P_h - 1$ non-zero elements; for ease of notation, we assume, as usually happens, that the non-zero elements of $\widetilde{\mathbf{H}}(n)$ are those corresponding to $n = 0, \ldots, \widetilde{P}-1$.

## B. Input-output relation

Denoting by $\mathbf{x}(n)$ the $N_T$-dimensional vector to be transmitted at discrete epoch $n$, it is easily shown that the received discrete-time signal at the output of the receive shaping filters is represented by the following $N_R$-dimensional vector

$$\mathbf{y}(n) = \sum_{\ell=0}^{\widetilde{P}-1} \widetilde{\mathbf{H}}(\ell)\mathbf{x}(n-\ell) + \mathbf{w}(n) \; , \tag{3}$$

with $\mathbf{w}(n)$ denoting the $N_R$-dimensional thermal noise vector at the output of the receive shaping filters. It is seen from (3) that the input-output relationship introduces intersymbol interference (ISI), thus implying that for SCM schemes properly equalization structures will be needed. Regarding the additive thermal noise, it is uncorrelated across antennas, i.e., the noise samples collected through different receive antennas are statistically independent: the vector $\mathbf{w}(n)$ is thus a complex zero-mean Gaussian random variable with covariance matrix $\sigma^2_w \mathbf{I}_{N_R}$, with $\sigma^2_w = 2\mathcal{N}_0\int_{-\infty}^{+\infty}|h_{\rm RX}(t)|^2 {\rm d}t$. Conversely, noise samples are in general correlated through time, i.e., we have

$$E\left[w_i(n)w_i^*(n-l)\right] = 2\mathcal{N}_0 r_{h_{\rm RX}}(lT_s) \; , \tag{4}$$

$\forall i = 1, \ldots, N_R$, where $w_i(n)$ denotes the $i$-th entry of the vector $\mathbf{w}(n)$, and $r_{h_{\rm RX}}(\tau) = \int_{-\infty}^{+\infty} h_{\rm RX}(t)h^*_{\rm RX}(t-\tau){\rm d}t$ denotes the correlation function of the receive shaping filter. It thus follows that, if we arrange $L$ consecutive noise vectors in an $(N_R \times L)$-dimensional matrix

$$\mathbf{W} = \left[\mathbf{w}(n)\; \mathbf{w}(n-1)\; \ldots, \mathbf{w}(n-L+1)\right] \; ,$$

we have that the entries of the matrix $\mathbf{W}$ are vertically uncorrelated (actually, independent) and horizontally correlated.

# III. Transceiver processing

Denote now by $\mathbf{s}$ a column vector containing the $L$ data-symbols – drawn either from a QAM constellation or from a Gaussian distribution, and with average energy $P_T$ – to be transmitted:

$$\mathbf{s} = [s_0, s_1, \ldots, s_{L-1}]^T \; . \tag{5}$$

We assume that $L = kM$, where $k$ is an integer and $M$, the multiplexing order, is the number of information symbols that are simultaneously transmitted by the $N_T$ transmit antennas in each symbol interval. In the following, we present three possible transceiver models.

## A. SCM with TDE

We refer to the discrete-time block-scheme reported in Fig. 1. The QAM symbols in vector $\mathbf{s}$ are fed to a serial-to-parallel (S/P) conversion block that splits them in $k$ distinct $M$-dimensional vectors $\check{\mathbf{s}}(1), \ldots, \check{\mathbf{s}}(k)$. These vectors are pre-coded using the $(N_T \times M)$-dimensional precoding matrix $\mathbf{Q}$; we thus obtain the $N_T$-dimensional vectors

$$\mathbf{x}(n) = \mathbf{Q}\check{\mathbf{s}}(n) \; , \qquad n = 1, \ldots, k \; .$$

The vectors $\mathbf{x}(n)$ are fed to a bank of $N_T$ identical shaping filters, converted to RF and transmitted.

At the receiver, after baseband-conversion, the $N_R$ received signals are passed through a bank of filters matched to those used for transmission and sampled at symbol-rate. We thus obtain the $N_R$-dimensional vectors $\mathbf{y}(n)$, which are passed through a postcoding matrix, that we denote by $\mathbf{D}$, of dimensions $(N_R \times M)$. Recalling that $\widetilde{\mathbf{H}}(n)$ is the matrix-valued FIR filter representing the composite channel impulse response (i.e., the convolution of the transmit filter, actual matrix-valued channel, and receive filter) it is easy to show, by virtue of the input-output relationship (3) that the generic $M$-dimensional vector at the output of the postcoding matrix, say $\widetilde{\mathbf{r}}(n)$, is written as

$$\widetilde{\mathbf{r}}(n) = \mathbf{D}^H\mathbf{y}(n) = \sum_{\ell=0}^{\widetilde{P}-1} \mathbf{D}^H\widetilde{\mathbf{H}}(\ell)\mathbf{Q}\check{\mathbf{s}}(n-\ell) + \mathbf{D}^H\mathbf{w}(n) \; . \tag{6}$$

So far, the choice of the pre-coding and post-coding beamforming matrices $\mathbf{Q}$ and $\mathbf{D}$ has been left unspecified. Since, as already said, FD structures are not practically realizable for mobile wireless applications due to hardware complexity and energy consumption issues, in this paper we will consider reduced-complexity hybrid analog-digital beamforming structures in order to approximate the desired FD beamforming strategies. In the following, we describe the considered FD beamforming structures, leaving to the next section the exposition of the algorithms for the design of the hybrid structures. Letting $\eta = \arg\max_{\ell=0,\ldots,\widetilde{P}-1}\left\{\left\|\widetilde{\mathbf{H}}(\ell)\right\|_{\mathrm{F}}\right\}$, we assume here that $\mathbf{Q}$ contains on its columns the left eigenvectors of the matrix $\widetilde{\mathbf{H}}(\eta)$ corresponding to the $M$ largest eigenvalues, and that the matrix $\mathbf{D}$ contains on its columns the corresponding right eigenvectors. Note that, due to the presence of ISI, the proposed pre-coding and post-coding structures are not optimal. Nevertheless, we make here this choice for the sake of simplicity, and resort to the use of an equalizer to cancel the effects of ISI. We will adopt a linear minimum mean square error (LMMSE) equalizer making a block processing of $\widetilde{P}$ consecutive received data vectors: to obtain a soft estimate of the data vector $\check{\mathbf{s}}(n)$, the $\widetilde{P}$ observables $\widetilde{\mathbf{r}}(n+\widetilde{P}-1)\ldots\widetilde{\mathbf{r}}(n)$ are stacked into a single $\widetilde{P}M$-dimensional vector, that we denote by $\widetilde{\mathbf{r}}_{\widetilde{P}}(n)$:

$$\widetilde{\mathbf{r}}_{\widetilde{P}}(n) = [\widetilde{\mathbf{r}}(n+\widetilde{P}-1)\ldots\widetilde{\mathbf{r}}(n)]^T \ .$$

Through ordinary algebra, it is easy to recognize that this vector can be expressed in the form

$$\widetilde{\mathbf{r}}_{\widetilde{P}}(n) = \mathbf{A}\check{\mathbf{s}}_{\widetilde{P}}(n) + \mathbf{B}\widetilde{\mathbf{w}}_{\widetilde{P}}(n) \ , \tag{7}$$

where $\check{\mathbf{s}}_{\widetilde{P}}(n)$ is an $M(2\widetilde{P}-1)$-dimensional vector containing the data symbols contributing to $\widetilde{\mathbf{r}}_{\widetilde{P}}(n)$, i.e.:

$$\check{\mathbf{s}}_{\widetilde{P}}(n) = [\check{\mathbf{s}}(n+\widetilde{P}-1)\ldots\check{\mathbf{s}}(n)\ldots\check{\mathbf{s}}(n-\widetilde{P}+1)]^T \ , \tag{8}$$

$\widetilde{\mathbf{w}}_{\widetilde{P}}(n)$ is the following $N_R\widetilde{P}$-dimensional noise vector

$$\widetilde{\mathbf{w}}_{\widetilde{P}}(n) = [\widetilde{\mathbf{w}}(n+\widetilde{P}-1)\ldots\widetilde{\mathbf{w}}(n)]^T \ , \tag{9}$$

and $\mathbf{A}$ and $\mathbf{B}$ are suitable matrices, of dimension $[M\widetilde{P}\times M(2\widetilde{P}-1)]$ and $[M\widetilde{P}\times N_R\widetilde{P}]$, respectively. The LMMSE estimator of the desired data vector $\widehat{\check{\mathbf{s}}}(n)$ is obtained through the following processing:

$$\widehat{\check{\mathbf{s}}}(n) = \mathbf{E}^H\widetilde{\mathbf{r}}_{\widetilde{P}}(n) \ , \tag{10}$$

where $\mathbf{E}$ is the $(\widetilde{P}M\times M)$-dimensional matrix LMMSE estimator. Its expression is given by [18]:

$$\mathbf{E} = (E[\widetilde{\mathbf{r}}_{\widetilde{P}}(n)\widetilde{\mathbf{r}}_{\widetilde{P}}(n)^H])^{-1}E[\widetilde{\mathbf{r}}_{\widetilde{P}}(n)\check{\mathbf{s}}(n)^H] \ , \tag{11}$$

where

$$\begin{aligned} E[\widetilde{\mathbf{r}}_{\widetilde{P}}(n)\widetilde{\mathbf{r}}_{\widetilde{P}}(n)^H] &= \tfrac{P_T}{M}\mathbf{A}\mathbf{A}^H + \mathbf{B}\mathbf{C}_{\widetilde{\mathbf{w}}_{\widetilde{\mathbf{P}}}}\mathbf{B}^H \ , \\ E[\widetilde{\mathbf{r}}_{\widetilde{P}}(n)\check{\mathbf{s}}(n)^H] &= \tfrac{P_T}{M}\mathbf{A}\mathbf{G}_{\widetilde{P}} \ . \end{aligned} \tag{12}$$

In (12), $\mathbf{C}_{\widetilde{\mathbf{w}}_{\widetilde{\mathbf{P}}}} = E[\widetilde{\mathbf{w}}_{\widetilde{P}}(n)\widetilde{\mathbf{w}}^H_{\widetilde{P}}(n)]$ is the covariance matrix of the noise vector $\widetilde{\mathbf{w}}_{\widetilde{P}}(n)$, while $\mathbf{G}_{\widetilde{P}}$ is an $[M\times M(2\widetilde{P}-1)]$-dimensional matrix defined as follows::

$$\mathbf{G}_{\widetilde{P}} = \left[\mathbf{0}_{[M\times M(\widetilde{P}-1)]} \quad \mathbf{I}_M \quad \mathbf{0}_{[M\times M(\widetilde{P}-1)]}\right]^T \ . \tag{13}$$

*Considerations on complexity.* Regarding processing complexity, we note that the computation of the equalization matrix $\mathbf{E}$ requires the inversion of the covariance matrix of the vector $\widetilde{\mathbf{r}}_{\widetilde{P}}(n)$, with a computational burden proportional to $(\widetilde{P}M)^3$; then, implementing (10) requires a matrix vector product, with a computational burden proportional to $(\widetilde{P}M^2)$; this latter task must be made $k$ times in order to provide the soft vector estimates for all values of $n=1,\ldots,k$.

## *B. SCM with FDE*

We now consider the case in which SCM is used in conjunction with a CP and FDE; we refer to the discrete-time block-scheme reported in Fig. 2. A cyclic prefix of length $CM$ is added at the beginning of the block $\mathbf{s}$ of $L=kM$ QAM symbols, so as to have the vector $\widetilde{\mathbf{s}}$ of length $(k+C)M$. As in the previous case, the vector $\widetilde{\mathbf{s}}$ is passed through a serial-to-parallel conversion with $M$ outputs, a precoding block (again expressed through the matrix $\mathbf{Q}$), a bank of $N_T$ transmit filters; then conversion to RF and transmission take place. At the receiver, after baseband-conversion, the $N_R$ received signals are passed through a bank of filters matched to the ones used for transmission and sampled at symbol-rate; then, the cyclic prefix is removed. We thus obtain the $N_R$-dimensional vectors $\widetilde{\mathbf{y}}(n)$, with $n=1,\ldots,k$, containing a noisy version of the *circular* convolution between the sequence $\widetilde{\mathbf{x}}(n)$ and $\widetilde{\mathbf{H}}(n)$ , i.e.:

$$\widetilde{\mathbf{y}}(n) = \widetilde{\mathbf{H}}(n)\circledast\widetilde{\mathbf{x}}(n) + \mathbf{w}(n) \ , \qquad n=1,\ldots,k \tag{14}$$

The vectors $\widetilde{\mathbf{y}}(n)$ are then processed by the post-coding matrix $\mathbf{D}$. The choice of the matrices $\mathbf{Q}$ and $\mathbf{D}$ is the same as that of the previous subsection (SCM with TDE), so we do not comment on it here. After post-coding beamforming, we obtain the $M$-dimensional vectors $\mathbf{r}(n) = \mathbf{D}^H\widetilde{\mathbf{y}}(n)$, with $n=1,\ldots,k$. These vectors go through an entry-wise FFT transformation on $k$ points; the $n$-th FFT coefficient, with $n=1,\ldots,k$, can be shown to be expressed as

$$\mathbf{R}(n) = \widetilde{\mathcal{H}}(n)\mathbf{X}(n) + \mathbf{W}(n) \ , \tag{15}$$

where $\widetilde{\mathcal{H}}(n)$ is an $(M\times N_T)$-dimensional matrix representing the $n$-th FFT coefficient of the matrix-valued sequence $\mathbf{D}^H\widetilde{\mathbf{H}}(n)$, and $\mathbf{X}(n)$ and $\mathbf{W}(n)$ are the $n$-th FFT coefficient of the sequences $\widetilde{\mathbf{x}}(n)$ and $\mathbf{D}^H\mathbf{w}(n)$, respectively. From (15), it is seen that, due to the presence of multiple antennas, and, thus, of the matrix-valued channel, the useful symbols reciprocally interfere and an equalizer is needed. (15) can be also shown to be expressed as:

$$\mathbf{R}(n) = \widetilde{\mathcal{H}}(n)\mathbf{Q}\widetilde{\mathbf{S}}(n) + \mathbf{W}(n) \ , \tag{16}$$

with $\widetilde{\mathbf{S}}(n)$ an $M$-dimensional vector representing the $n$-th FFT coefficient of the vector-valued sequence $\widetilde{\mathbf{s}}(n)$.[2] We denote by $\mathbf{E}(n)$ the $(M\times M)$-dimensional equalization matrix, and a zero-forcing approach is adopted, thus implying that $\mathbf{E}^H(n) = (\widetilde{\mathcal{H}}(n)\mathbf{Q})^{-1}$. The output of the equalizer is written as

$$\mathbf{Z}(n) = \mathbf{E}^H(n)\mathbf{R}(n) = \widetilde{\mathbf{S}}(n) + (\widetilde{\mathcal{H}}(n)\mathbf{Q})^{-1}\mathbf{W}(n) \ .$$

Then, the vectors $\mathbf{Z}(n)$ go through an entry-wise IFFT transformation on $k$ points. It can be shown that the $n$-th IFFT coefficient of the vector $\mathbf{Z}(n)$ can be expressed as:

$$\mathbf{z}(n) = \widetilde{\mathbf{s}}(n) + \left[\mathbf{I}_M\otimes[\mathbf{D}_{\mathrm{IFFT}}]_{:,n}\right]\mathbf{N}_{\mathrm{stacked}} \ , \tag{17}$$

where $[\mathbf{D}_{\mathrm{IFFT}}]_{:,n}$ is the $n$-th column of the isometric IFFT matrix $\mathbf{D}_{\mathrm{IFFT}}$, whose $(m,l)$-th element is given by

$$\mathbf{D}_{\mathrm{IFFT}}(m,l) = \frac{1}{\sqrt{k}}e^{j2\pi\frac{(m-1)(l-1)}{k}} \ ,$$

[2]We used here the relation $\mathbf{X}(n) = \mathbf{Q}\widetilde{\mathbf{S}}(n)$.

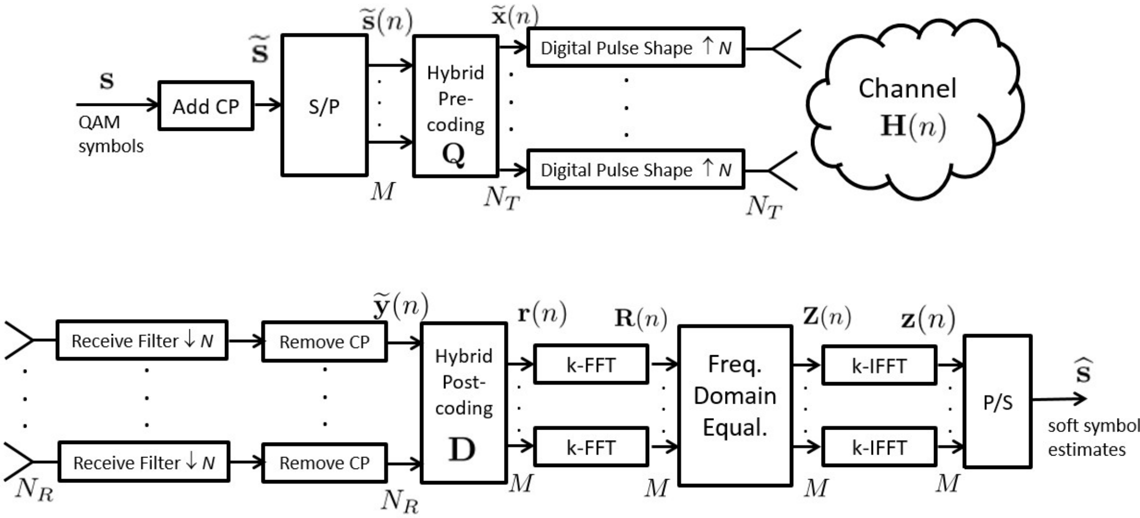


Figure 2. Transceiver block-scheme for SCM with cyclic prefix, FFT-based processing and FDE.

and $\mathbf{N}_{\text{stacked}}$ is the $kM$-dimensional vector containing the stacked vectors $(\widetilde{\mathcal{H}}(1)\mathbf{Q})^{-1}\mathbf{W}(1), \ldots, (\widetilde{\mathcal{H}}(k)\mathbf{Q})^{-1}\mathbf{W}(k)$.

*Considerations on complexity.* Looking at the scheme in Fig. 2, the computational burden of the considered transceiver architecture is the following. $2M$ FFTs of length $k$ are required, with a complexity proportional to $2Mk\log_2 k$; in order to compute the zero-forcing matrix, the FFT of the matrix-valued sequence $\widetilde{\mathcal{H}}(n)$ must be computed, with a complexity proportional to $MN_T(k\log_2 k)$; computation of the matrix $(\widetilde{\mathcal{H}}(n)\mathbf{Q})$ and of its inverse, for $n = 1, \ldots, k$, finally requires a computational burden proportional to $k(N_T M^2 + M^3)$.

It can be easily seen that the complexity of the FDE scheme is lower than that of the TDE scheme.

### *C. Transceiver model - OFDM*

Finally, we consider, for benchmarking purposes, the MIMO-OFDM discrete-time block-scheme reported in Fig. 3. Differently from previous schemes, we have explicitly separated the baseband digital beamforming from its analog counterparts; such a separation is needed in order to keep down system complexity, and to explicitly point out that while baseband FD beamforming is made on a "per-subcarrier" basis, the analog beamformer jointly process the entire signal bandwidth, i.e., all the subcarriers are treated uniformly. In Fig. 3, $N_T^{\text{RF}}$ and $N_R^{\text{RF}}$ RF chains are considered at the transmitter and at the receiver, and we have $M \leq N_T^{\text{RF}} \leq N_T$ and $M \leq N_R^{\text{RF}} \leq N_R$. Notice also that the choice $N_T^{\text{RF}} = N_T$ and $N_R^{\text{RF}} = N_R$ results in a non-hybrid, FD beamforming.

Each OFDM symbol is assumed to be made of $L = kM$ QAM data symbols; after S/P conversion, the data symbols are split in $k$ distinct $M$-dimensional vectors $\overline{\mathbf{S}}(1), \ldots, \overline{\mathbf{S}}(k)$. These vectors are pre-coded through the $(N_T^{\text{RF}} \times M)$-dimensional digital precoding matrices $\mathbf{Q}_{\text{BB}}(1), \ldots, \mathbf{Q}_{\text{BB}}(n)$, thus yielding the vectors $\overline{\mathbf{X}}(n) = \mathbf{Q}_{\text{BB}}(n)\overline{\mathbf{S}}(n)$ – note that we are here assuming that the digital pre-coding matrix is not constant over all the sub-carriers [19]. These vectors then go through an entry-wise IFFT transformation on $k$ points; we denote by $\overline{\mathbf{x}}(n)$ the $M$-dimensional transformed vectors, with $n = 1, \ldots, k$. A CP of length $C$ is added at the beginning of the block so that we have the following sequence of $N_T$-dimensional vectors:

$$\overline{\mathbf{x}}^{\text{CP}}(n) = \begin{cases} \overline{\mathbf{x}}(n+k-C) \,, n = 1, \ldots, C \,, \\ \overline{\mathbf{x}}(n-C) \,, \qquad n = C+1, \ldots, C+k \,. \end{cases} \tag{18}$$

The vectors $\overline{\mathbf{x}}^{\text{CP}}(n)$ are precoded through the $(N_T \times N_T^{\text{RF}})$-dimensional analog precoding matrix $\mathbf{Q}_{\text{RF}}$, thus yielding the vectors $\overline{\mathbf{v}}(n) = \mathbf{Q}_{\text{RF}}\overline{\mathbf{x}}^{\text{CP}}(n)$. The vectors $\overline{\mathbf{v}}(n)$ are passed through a bank of $N_T$ transmit filters, converted to RF and transmitted. At the receiver, after baseband-conversion, the $N_R$ received signals are passed through a bank of filters matched to the ones used for transmission and sampled at symbol-rate; then, they are post-coded through the $(N_R \times N_R^{\text{RF}})$-dimensional analog precoding matrix $\mathbf{D}_{\text{RF}}$ and the cyclic prefix is removed. We thus obtain the following $N_R^{\text{RF}}$-dimensional vectors $\overline{\mathbf{y}}(n)$, with $n = 1, \ldots, k$:

$$\overline{\mathbf{y}}(n) = \mathbf{D}_{\text{RF}}^H \left[\widetilde{\mathbf{H}}(n) \circledast \mathbf{Q}_{\text{RF}}\overline{\mathbf{x}}(n)\right] + \mathbf{D}_{\text{RF}}^H \mathbf{w}(n) \,, \tag{19}$$

with $\widetilde{\mathbf{H}}(n)$ denoting again the matrix-valued FIR filter representing the composite channel impulse response (i.e., the convolution of the transmit filter, actual matrix-valued channel and receive filter). These vectors go through an entry-wise FFT transformation on $k$ points; the $n$-th FFT coefficient, with $n = 1, \ldots, k$, can be shown to be expressed as

$$\overline{\mathbf{Y}}(n) = \mathbf{D}_{\text{RF}}^H \overline{\mathcal{H}}(n)\mathbf{Q}_{\text{RF}}\mathbf{Q}_{\text{BB}}(n)\overline{\mathbf{S}}(n) + \mathbf{D}_{\text{RF}}^H \overline{\mathbf{W}}(n) \,, \tag{20}$$

where $\overline{\mathcal{H}}(n)$ is an $(N_R \times N_T)$-dimensional matrix representing the $n$-th FFT coefficient of the matrix-valued sequence $\widetilde{\mathbf{H}}(n)$, and $\overline{\mathbf{W}}(n)$ is the $n$-th FFT coefficient of the sequence $\mathbf{w}(n)$, respectively. The vectors $\overline{\mathbf{Y}}(n)$ are then processed by the digital post-coding matrix $\mathbf{D}_{\text{BB}}(n)$; we thus obtain the $M$-dimensional vectors

$$\begin{aligned} \overline{\mathbf{R}}(n) = {} & \mathbf{D}_{\text{BB}}^H(n)\mathbf{D}_{\text{RF}}^H \overline{\mathcal{H}}(n)\mathbf{Q}_{\text{RF}}\mathbf{Q}_{\text{BB}}(n)\overline{\mathbf{S}}(n) + \\ & \mathbf{D}_{\text{BB}}^H(n)\mathbf{D}_{\text{RF}}^H \overline{\mathbf{W}}(n) \,, \quad n = 1, \ldots, k \,. \end{aligned} \tag{21}$$

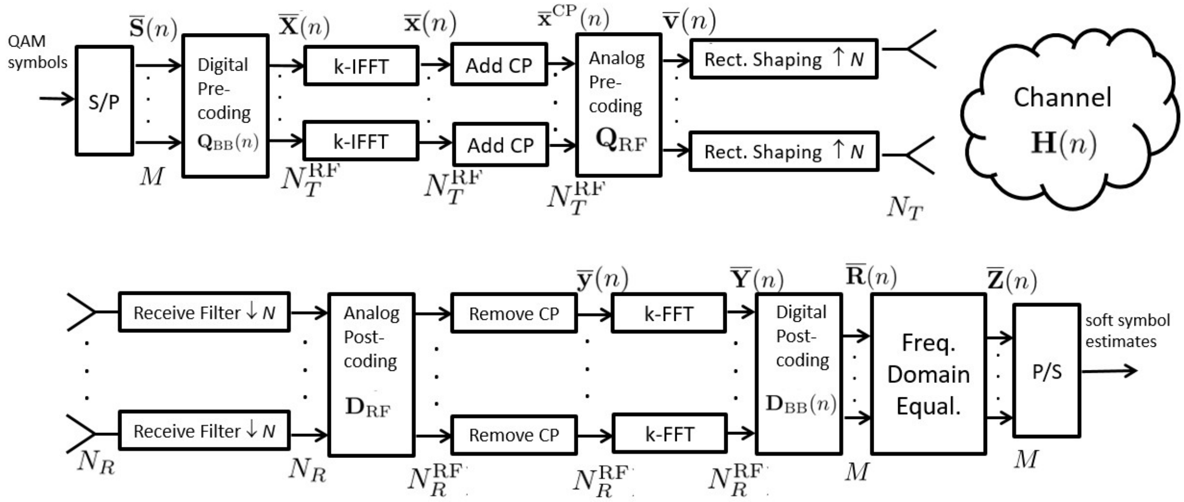


Figure 3. Transceiver block-scheme for OFDM with FDE.

From (20), it is seen that, due to the presence of multiple antennas, and, thus, of the matrix-valued channel, the useful symbols reciprocally interfere and thus an equalizer is needed. Denoting by $\overline{\mathbf{E}}(n)$ the $(M \times M)$-dimensional equalization matrix, and using a zero-forcing approach, it can be seen that $\overline{\mathbf{E}}^H(n) = (\mathbf{D}_{\mathrm{BB}}^H(n)\mathbf{D}_{\mathrm{RF}}\overline{\mathcal{H}}(n)\mathbf{Q}_{\mathrm{RF}}\mathbf{Q}_{\mathrm{BB}}(n))^+$, where $(\cdot)^+$ denotes the Moore-Penrose pseudoinverse. The output of the equalizer can be shown to be expressed as:

$$\begin{aligned}\overline{\mathbf{Z}}(n) &= \overline{\mathbf{E}}(n)^H\overline{\mathbf{R}}(n) = \overline{\mathbf{S}}(n) + \\ &(\mathbf{D}_{\mathrm{BB}}(n)^H\mathbf{D}_{\mathrm{RF}}^H\overline{\mathcal{H}}(n)\mathbf{Q}_{\mathrm{RF}}\mathbf{Q}_{\mathrm{BB}}(n))^+\mathbf{D}_{\mathrm{BB}}(n)^H\mathbf{W}(n)\ .\end{aligned} \tag{22}$$

After P/S conversion we finally obtain the soft estimates of the transmitted symbols.

## IV. Hybrid architecture design

We now detail the low-complexity hybrid beamforming structures. We first deal with the case of SCM, and then will examine the MIMO-OFDM case.

### *A. Hybrid beamforming for SCM schemes*

In order to reduce hardware complexity with respect to the FD beamforming, in hybrid structures the $(N_T \times M)-$dimensional pre-coding matrix is written as $\mathbf{Q} = \mathbf{Q}_{\mathrm{RF}}\mathbf{Q}_{\mathrm{BB}}$, where $\mathbf{Q}_{\mathrm{RF}}$ is the $(N_T \times N_T^{RF})$-dimensional RF precoding matrix and $\mathbf{Q}_{\mathrm{BB}}$ is the $(N_T^{RF} \times M)-$dimensional baseband precoding matrix. Since the RF precoder is implemented using phase shifters, the entries of the matrix $\mathbf{Q}_{RF}$ have all the same magnitude (equal to $\frac{1}{\sqrt{N_T}}$), and just differ for the phase. Now, denoting by $\mathbf{Q}^{\mathrm{opt}}$ the $(N_T \times M)-$dimensional FD beamforming that we would use in the situation of no hardware complexity constraints, the matrices $\mathbf{Q}_{\mathrm{RF}}$ and $\mathbf{Q}_{\mathrm{BB}}$ can be found by using the Frobenius norm as a distance metric and solving the following optimization problem:

$$\begin{aligned}&(\mathbf{Q}_{\mathrm{RF}}^*, \mathbf{Q}_{\mathrm{BB}}^*) = \underset{\mathbf{Q}_{\mathrm{RF}},\mathbf{Q}_{\mathrm{BB}}}{\arg\min}\, ||\mathbf{Q}^{\mathrm{opt}} - \mathbf{Q}_{\mathrm{RF}}\mathbf{Q}_{\mathrm{BB}}||_F \\ &\text{subject to} \qquad |\mathbf{Q}_{\mathrm{RF}}(i,j)| = \frac{1}{\sqrt{N_T}}\ , \quad \forall i,j \\ &\qquad\qquad\qquad ||\mathbf{Q}_{\mathrm{RF}}\mathbf{Q}_{\mathrm{BB}}||_F^2 \leq M\ .\end{aligned} \tag{23}$$

Similarly, with regard to the design of the post-coding beamforming matrix, the optimal FD beamformer $\mathbf{D}^{\mathrm{opt}}$ that we would use in case of no hardware complexity constraints is approximated by the product $\mathbf{D}_{\mathrm{RF}}\mathbf{D}_{\mathrm{BB}}$, where $\mathbf{D}_{\mathrm{RF}}$ is the $(N_R \times N_R^{RF})-$dimensional RF post-coding matrix and $\mathbf{D}_{\mathrm{BB}}$ is the $(N_R^{RF} \times M)-$dimensional baseband post-coding matrix. The entries of the RF post-coder $\mathbf{D}_{\mathrm{RF}}$ are constrained to have norm equal to $\frac{1}{\sqrt{N_R}}$. The matrices $\mathbf{D}_{\mathrm{RF}}$ and $\mathbf{D}_{\mathrm{BB}}$ can be then found solving the following optimization problem

$$\begin{aligned}&(\mathbf{D}_{\mathrm{RF}}^*, \mathbf{D}_{\mathrm{BB}}^*) = \underset{\mathbf{D}_{\mathrm{RF}},\mathbf{D}_{\mathrm{BB}}}{\arg\min}\, ||\mathbf{D}^{\mathrm{opt}} - \mathbf{D}_{\mathrm{RF}}\mathbf{D}_{\mathrm{BB}}||_F \\ &\text{subject to} \qquad |\mathbf{D}_{\mathrm{RF}}(i,j)| = \frac{1}{\sqrt{N_R}}\ , \quad \forall i,j\ .\end{aligned} \tag{24}$$

It is easy to show that optimization problems (23) and (24) are not convex optimization problem; inspired by [20], we thus resort to the Block Coordinate Descent for Subspace Decomposition (BCD-SD) algorithm, that basically is based on a sequential iterative update of the analog part and of the baseband part of the beamformers. The algorithm's recipe is reported in Algorithm 1.

### *B. Hybrid beamforming for the MIMO-OFDM transceiver*

We now consider the issue of beamformer design for the MIMO-OFDM transceiver. From (21) it is seen that the optimal pre-coders and post-coders for the detection of the data vector $\overline{\mathbf{S}}(n)$ are given by the left and right singular vectors associated to the $M$ largest eigenvalues of the matrix $\overline{\mathcal{H}}(n)$, respectively. We will denote these optimal beamformers as $\mathbf{Q}^{\mathrm{opt}}(n)$ and $\mathbf{D}^{\mathrm{opt}}(n)$, respectively; differently from what happens for the SCM transceivers, these beamformers are now carrier dependent. Our aim is to approximate the optimal

**Algorithm 1** Block Coordinate Descent for Subspace Decomposition Algorithm for Hybrid Beamforming

Initialize $I_{\max}$ and set $i = 0$
Set arbitrary $\mathbf{Q}_{\mathrm{RF},0}$ and $\mathbf{D}_{\mathrm{RF},0}$
**repeat**
  Update $\mathbf{Q}_{\mathrm{BB,i+1}} = \left(\mathbf{Q}_{\mathrm{RF,i}}^{H}\mathbf{Q}_{\mathrm{RF,i}}\right)^{-1}\mathbf{Q}_{\mathrm{RF,i}}^{H}\mathbf{Q}^{\mathrm{opt}}$
  and $\mathbf{D}_{\mathrm{BB,i+1}} = \left(\mathbf{D}_{\mathrm{RF,i}}^{H}\mathbf{D}_{\mathrm{RF,i}}\right)^{-1}\mathbf{D}_{\mathrm{RF,i}}^{H}\mathbf{D}^{\mathrm{opt}}$
  Set $\phi_i = \mathbf{Q}^{\mathrm{opt}}\mathbf{Q}_{\mathrm{BB,i+1}}^{H}\left(\mathbf{Q}_{\mathrm{BB,i+1}}\mathbf{Q}_{\mathrm{BB,i+1}}^{H}\right)^{-1}$
  and $\psi_i = \mathbf{D}^{\mathrm{opt}}\mathbf{D}_{\mathrm{BB,i+1}}^{H}\left(\mathbf{D}_{\mathrm{BB,i+1}}\mathbf{D}_{\mathrm{BB,i+1}}^{H}\right)^{-1}$
  Update $\mathbf{Q}_{\mathrm{RF,i}} = \frac{1}{\sqrt{N_T}}e^{j\phi_i}$
  and $\mathbf{D}_{\mathrm{RF,i}} = \frac{1}{\sqrt{N_R}}e^{j\psi_i}$
  Set $i = i + 1$
**until** convergence or $i = I_{\max}$

pre-coder $\mathbf{Q}^{\mathrm{opt}}(n)$ with the product $\mathbf{Q}_{\mathrm{RF}}\mathbf{Q}_{\mathrm{BB}}(n)$, and the optimal post-coder $\mathbf{D}^{\mathrm{opt}}(n)$ with the product $\mathbf{D}_{\mathrm{RF}}\mathbf{D}_{\mathrm{BB}}(n)$. Now, letting [19]

$$\begin{aligned}
\mathbf{Q}^{\mathrm{opt}} &= [\mathbf{Q}^{\mathrm{opt}}(1), \ldots, \mathbf{Q}^{\mathrm{opt}}(k)] \quad \in \mathbb{C}^{N_T \times kM}\ , \\
\mathbf{D}^{\mathrm{opt}} &= [\mathbf{D}^{\mathrm{opt}}(1), \ldots, \mathbf{D}^{\mathrm{opt}}(k)] \quad \in \mathbb{C}^{N_R \times kM}\ , \\
\mathbf{Q}_{\mathrm{BB}} &= [\mathbf{Q}_{\mathrm{BB}}(1), \ldots, \mathbf{Q}_{\mathrm{BB}}(k)] \quad \in \mathbb{C}^{N_T^{RF} \times kM}\ , \\
\mathbf{D}_{\mathrm{BB}} &= [\mathbf{D}_{\mathrm{BB}}(1), \ldots, \mathbf{D}_{\mathrm{BB}}(k)] \quad \in \mathbb{C}^{N_R^{RF} \times kM}\ ,
\end{aligned}$$

the hybrid beamformer design amount to solving the following two constrained optimization problems

$$\begin{aligned}
(\mathbf{Q}_{\mathrm{RF}}^{*}, \mathbf{Q}_{\mathrm{BB}}^{*}) &= \underset{\mathbf{Q}_{\mathrm{RF}}, \mathbf{Q}_{\mathrm{BB}}}{\arg\min} ||\mathbf{Q}^{\mathrm{opt}} - \mathbf{Q}_{\mathrm{RF}}\mathbf{Q}_{\mathrm{BB}}||_F \\
\text{subject to} \quad & |\mathbf{Q}_{\mathrm{RF}}(i,j)| = \tfrac{1}{\sqrt{N_T}}\ , \\
& \|\mathbf{Q}_{\mathrm{RF}}\mathbf{Q}_{\mathrm{BB,k}}\|_F^2 \le kM\ ,
\end{aligned} \tag{25}$$

and

$$\begin{aligned}
(\mathbf{D}_{\mathrm{RF}}^{*}, \mathbf{D}_{\mathrm{BB}}^{*}) &= \underset{\mathbf{D}_{\mathrm{RF}}, \mathbf{D}_{\mathrm{BB}}}{\arg\min} ||\mathbf{D}^{\mathrm{opt}} - \mathbf{D}_{\mathrm{RF}}\mathbf{D}_{\mathrm{BB}}||_F \\
\text{subject to} \quad & |\mathbf{D}_{\mathrm{RF}}(i,j) = \tfrac{1}{\sqrt{N_R}}\ .
\end{aligned} \tag{26}$$

The above optimization problems have the same structure as problems in (23) and (24), and can thus be solved through a straightforward application of the BCD-SD algorithm. We do not explicitly report here the full details of the algorithm for the sake of brevity.

## V. Computation of the achievable spectral efficiency

As a figure of merit to compare the different transceiver architectures we will use the ASE, that is the maximum achievable spectral efficiency with the constraint of arbitrarily small BER and of pre-fixed modulation type. The ASE takes the particular constellation and signaling parameters into consideration, so it does not qualify as a normalized capacity measure; (it is derived from the *constrained capacity*). We focus here on ergodic rates so the ASE is computed given the channel realization and averaged over it (remember that we are assuming perfect channel state information at the receiver). The spectral efficiency $\rho$ of any practical coded modulation system operating at a low packet error rate is upper bounded by the ASE, i.e., $\rho \le \mathrm{ASE}$, where

$$\mathrm{ASE} = \frac{1}{T_{\mathrm{s}}W}\lim_{L\to\infty}\frac{1}{L}E_{\widetilde{\mathbf{H}}}\left[I(\mathbf{s};\hat{\mathbf{s}}|\widetilde{\mathbf{H}})\right]\ \mathrm{bit/s/Hz} \tag{27}$$

$I(\mathbf{s};\hat{\mathbf{s}}|\tilde{\mathbf{H}})$ being the mutual information (given the channel realization) between the transmitted data symbols and their soft estimates, $T_{\mathrm{s}}$ the symbol interval, and $W$ the signal bandwidth (as specified in Section VI). Although not explicitly reported, for notational simplicity, the ASE in (27) depends on the Signal-to-Interference plus Noise Ratio (SINR).

The computation of the mutual information requires the knowledge of the channel conditional probability density function (pdf) $p(\hat{\mathbf{s}}|\mathbf{s},\tilde{\mathbf{H}})$. As already said, it can be numerically computed by adopting the simulation-based technique described in [13] once the channel at hand is finite-memory and the optimal detector for it is available. In addition, only the optimal detector for the actual channel is able to achieve the ASE in (27).

In both transceiver models described in Section III the soft symbol estimates can be expressed in the form

$$\widehat{\mathbf{s}}(n) = \mathbf{C}\mathbf{s}(n) + \sum_{\ell\neq 0}\mathbf{C}_\ell\mathbf{s}(n-\ell) + \mathbf{z}(n) \tag{28}$$

i.e., as a linear transformation (through matrix $\mathbf{C}$, which eventually is zero in the FDE case with zero-forcing equalization) of the desired QAM data symbols, plus a linear combination of the interfering data symbols and the colored noise $\mathbf{z}(n)$ having a proper covariance matrix. The optimal receiver has a computational complexity which is out of reach and for this reason we consider much simpler linear suboptimal receivers. Hence, we are interested in the achievable performance when using suboptimal low-complexity detectors. We thus resort to the framework described in [13, Section VI]. We compute proper lower bounds on the mutual information (and thus on the ASE) obtained by substituting $p(\hat{\mathbf{s}}|\mathbf{s},\tilde{\mathbf{H}})$ in the mutual information definition with an arbitrary auxiliary channel law $q(\hat{\mathbf{s}}|\mathbf{s},\tilde{\mathbf{H}})$ with the same input and output alphabets as the original channel (mismatched detection [13])—the more accurately the auxiliary channel approximates the actual one, the closer the bound is. If the auxiliary channel law can be represented/described as a finite-state channel, the pdfs $q(\hat{\mathbf{s}}|\mathbf{s},\tilde{\mathbf{H}})$ and $q_p(\hat{\mathbf{s}}|\tilde{\mathbf{H}}) = \sum_{\mathbf{s}} q(\hat{\mathbf{s}}|\mathbf{s},\tilde{\mathbf{H}})P(\mathbf{s})$ can be computed, this time, by using the optimal maximum a posteriori symbol detector for that auxiliary channel [13]. This detector, that is clearly suboptimal for the actual channel, has at its input the sequence $\hat{\mathbf{s}}$ generated by simulation *according to the actual channel model* (for details, see [13]). If we change the adopted receiver (or, equivalently, if we change the auxiliary channel) we obtain different lower bounds on the constrained capacity but, in any case, these bounds are *achievable* by those receivers, according to mismatched detection theory [13]. We thus say, with a slight abuse of terminology, that the computed lower bounds are the ASE values of the considered channel when those receivers are employed. This technique thus allows us to take reduced-complexity receivers into account. In fact, it is sufficient to consider an auxiliary channel which is a simplified version of the actual channel in the sense that only a portion of the actual channel memory and/or a limited number of impairments are present. In particular, we will use the auxiliary channel law (28), where the sum of the interference and the thermal noise $\mathbf{z}(n)$ is assimilated to Gaussian noise with a proper covariance matrix.

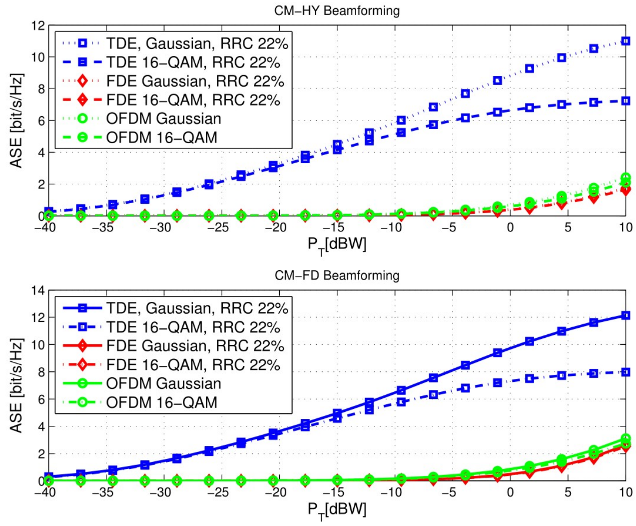


Figure 4. ASE versus transmit power; comparison of TDE, FDE and OFDM, with finite and infinite modulation cardinality and with comparison of hybrid (CM-HY) and digital (CM-FD) beamforming. Parameters: $M = 2$; $d = 30$ m $N_R \times N_T = 10 \times 50$.

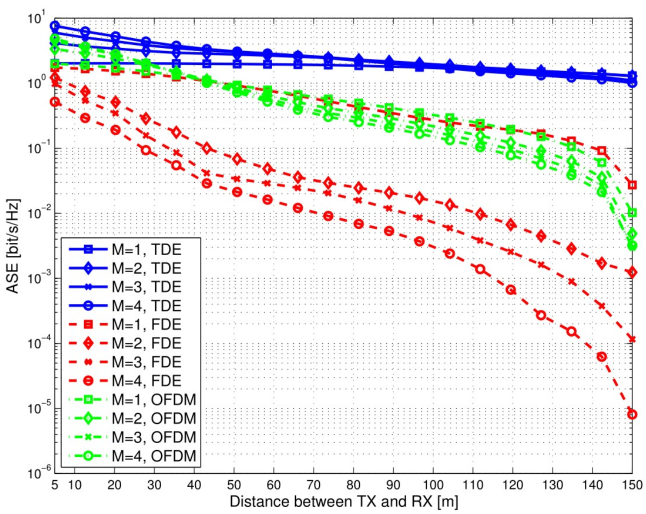


Figure 5. ASE versus distance; impact of multiplexing order, comparison of hybrid (CM-HY) and digital (CM-FD) beamforming with TDE, FDE and OFDM. Parameters: 4-QAM modulation; $P_T = 0$ dBW; $N_R \times N_T = 10 \times 50$.

The transceiver models are compared in terms of ASE without taking into account specific coding schemes, being understood that, with a properly designed channel code, the information-theoretic performance can be closely approached.

## VI. Numerical Results

In our simulation setup, we consider a communication bandwidth of $W = 500$ MHz centered over a mmWave carrier frequency. The MIMO propagation channel, described in Section II, has been generated according to the statistical procedure detailed in [17]. The additive thermal noise is assumed to have a power spectral density of -174 dBm/Hz, while the front-end receiver is assumed to have a noise figure of 3 dB. We start by studying, in the following figures, the ASE for varying values of the transmit power $P_T$, of the

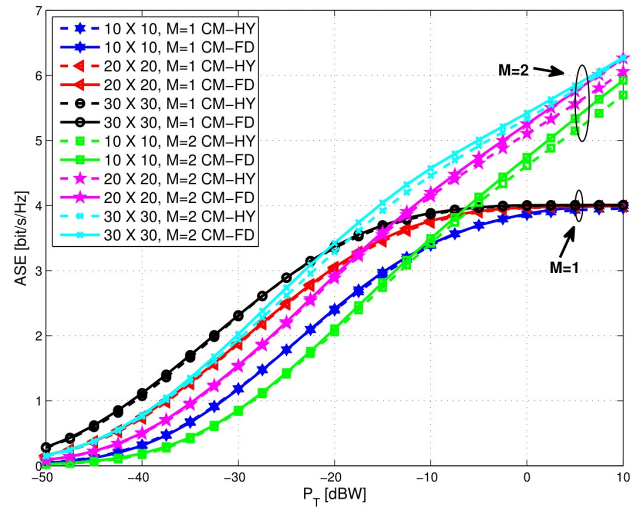


Figure 6. ASE versus transmit power; impact of array size, multiplexing order and comparison of hybrid (CM-HY) and digital (CM-FD) beamforming. Parameters: 16-QAM modulation; $d = 30$ m; varying $N_R \times N_T$.

distance $d$ between the transmitter and the receiver, of the number of transmit and receive antennas, of the multiplexing order $M$, and for the case in which the Root Raised Cosine (RRC) pulse with roll off factor 0.22 is adopted. For this waveform, we define the bandwidth as the frequency range such that out-of-band emissions are 40 dB below the maximum in-band value of the Fourier transform of the pulse. For the considered communication bandwidth of $W = 500$ MHz, we found that the symbol interval $T_s$ is 1.98 ns, for the case in which we consider its truncated version to the interval $[-4T_s, 4T_s]$. The reported results are to be considered as an ideal benchmark for the ASE since we are neglecting the interference.[3] Hybrid pre-coding and post-coding, with $M$ RF chains at the transmitter and at the receiver, is considered, also in comparison to FD structures. Fig. 4 reports the ASE[4] of SCM-TDE, SCM-FDE and MIMO-OFDM using finite and infinite modulation cardinality versus the transmit power $P_T$ (varying in the range $[-50, 10]$ dBW), while instead in Fig. 5 the ASE for the three considered access schemes is reported versus the distance $d$ between the transmitter and the receiver, assuming that the transmit power is $P_T = 0$ dBW. While Fig. 4 contains a comparison between the 16-QAM modulation scheme and the case of Gaussian-distributed data symbols, Fig. 5 focuses on the case of 4-QAM modulation and studies the impact of the multiplexing order $M$. Both these figures consider a link with $N_R \times N_T = 10 \times 50$.

We can see that the SCM-TDE performance is much better than the MIMO-OFDM and the SCM-FDE ones, with MIMO-OFDM slightly outperforming the SCM-FDE scheme. Figs. 6 focuses on the SCM-TDE scheme and reports the ASE versus the transmitted power $P_T$ (assuming a link length $d > 30$ m), studying the impact of the multiplexing order and of the size

[3]We note however that being mmWave systems mainly noise-limited rather than interference limited, the impact of this assumption on the obtained results is very limited.

[4]Of course, the achievable rates in bit/s can be immediately obtained by multiplying the ASE by the communication bandwidth $W = 500$ MHz.

of the antenna arrays, while Fig. 7 reports, again for the SCM-TDE scheme, the ASE versus the link length (assuming $P_T = 0$ dBW), studying the impact of the modulation cardinality and of the size of the antenna arrays. Inspecting the figures, the following remarks are in order:

- Results, in general, as it is obvious, improve for increasing transmit power, for decreasing distance $d$ between transmitter and receiver and for increasing values of the number of transmit and receive antennas.
- In particular, a good performance can be attained for distances up to 100 m, whereas for $d > 100$ m we have a steep degradation of the ASE. In this region, all the advantages given by increasing the modulation cardinality or the number of antennas are essentially lost or reduced at very small values. Of course, this performance degradation may be compensated by increasing the transmit power.
- Regarding the multiplexing index $M$, it is interesting to note from Fig. 5 that for short distances the system benefits from a large multiplexing order, while, for large distances (which essentially correspond to low signal-to-noise ratio), the ASE corresponding to $M = 1$ is larger than that corresponding to the choice $M > 1$. This behavior is in agreement with the well-known result that for low signal-to-noise ratio there is no advantage in increasing the multiplexing order.
- For a reference distance of 30 m (which will be a typical one in small-cell 5G mmWave deployments for densely crowded areas), a transmit power around 0 dBW is enough to grant good performance and to benefit from the advantages of increased modulation cardinality, size of the antenna array, and multiplexing order.

We now proceed to showing BER results. In Figs 8, 9 and 10 we report the BER results respectively of 16QAM SCM-TDE, SCM-FDE and MIMO-OFDM when employing low-density-parity-check (LDPC) codes of rate equal to 1/2 and 9/10, in order to show how practical (i.e., finite-length and not *ad hoc* designed) codes perform in one realization of the considered scenario, which entails $M = 2$, $d = 30$ m, $N_R \times N_T = 10 \times 50$. The parameters of the codes are reported in Table I where $r_c$ denotes the rate of the code and the degree distributions of variable and check nodes are provided by giving the fraction $a_i$ ($\sum_i a_i = 1$) of degree $i$ nodes. In any case, the codeword length is $N = 64800$ bits, and the decoder iterations are limited to 40. These codes were designed for low intersymbol interference (ISI) channels, and, despite not specifically designed for these systems, they closely approach the provided ASE lower bounds. Since with $M = 2$ the two multiplexed streams perform differently, the code rates on each stream should be tailored accordingly.

## VII. Conclusion

This paper has provided a comparison between single-carrier modulation schemes and conventional OFDM for a MIMO link operating at mmWave frequencies. In particular, two SCM techniques have been considered, SCM-TDE and SCM-FDE, and these transceivers have been compared with the MIMO-OFDM scheme. Our analysis has taken into account both the peculiarity of the channel matrix at mmWave frequencies (a clustered model has been adopted), and the adoption of hybrid analog/digital beamforming structures. Results have shown that the SCM-TDE structure achieves superior performance with respect to the other two competing schemes, with the MIMO-OFDM slightly outperforming the SCM-FDE scheme. The present study can be generalized and strengthened in many directions. First of all, the considered analysis might be applied in a multiuser environment; then, since, as already discussed, the reduced wavelength of mmWave frequencies permits installing arrays with many antennas in small volumes, an analysis, possibly through asymptotic analytic considerations, of the very large number of antennas regime could also be made. Last, but not least, energy-efficiency considerations should also be made: both the ASE and the transceiver power consumption increase for increasing transmit power and increasing size of the antenna

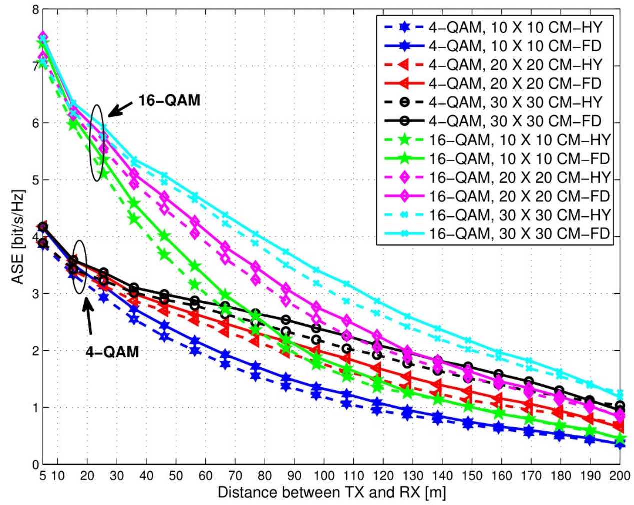


Figure 7. ASE versus distance; impact of modulation cardinality, array size and comparison of hybrid (CM-HY) and digital (CM-FD) beamforming. Parameters: $P_T = 0$ dBW; $M = 2$; varying $N_R \times N_T$.

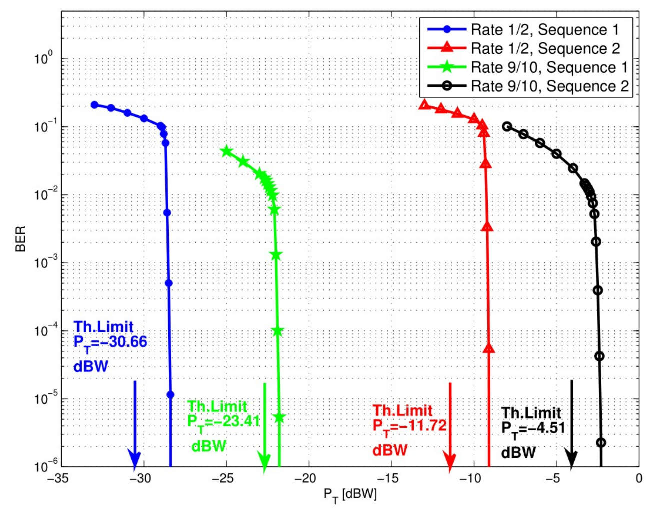


Figure 8. BER of TDE for 16QAM, d=30 m, $M$=2, $N_R \times N_T = 10 \times 50$.

Table I
CODE RATES AND DEGREE DISTRIBUTIONS OF THE EMPLOYED LDPC CODES.

| $r_c$ | variable node distribution | check node distribution |
|---|---|---|
| 1/2 | $a_2 = 0.499985$ $a_3 = 0.3$ $a_8 = 0.200015$ | $a_7 = 0.999815$ $a_8 = 0.000185185$ |
| 9/10 | $a_2 = 0.0999846$ $a_3 = 0.8$ $a_4 = 0.1111111$ | $a_{30} = 0.999691$ $a_{31} = 0.000308642$ |

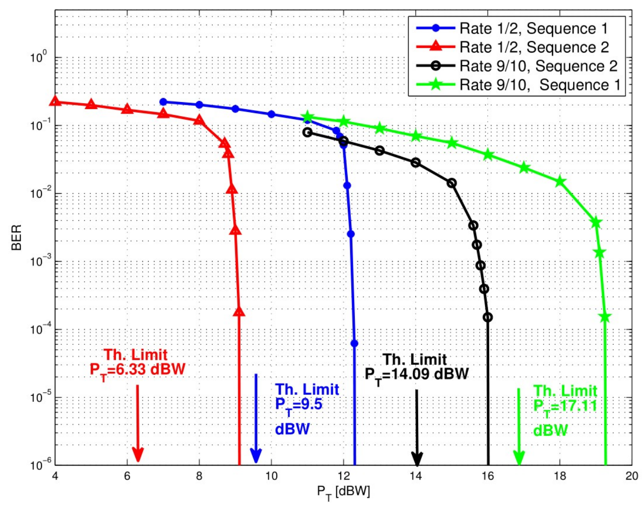


Figure 9. BER of FDE for 16QAM, d=30 m, $M$=2, $N_R \times N_T = 10 \times 50$.

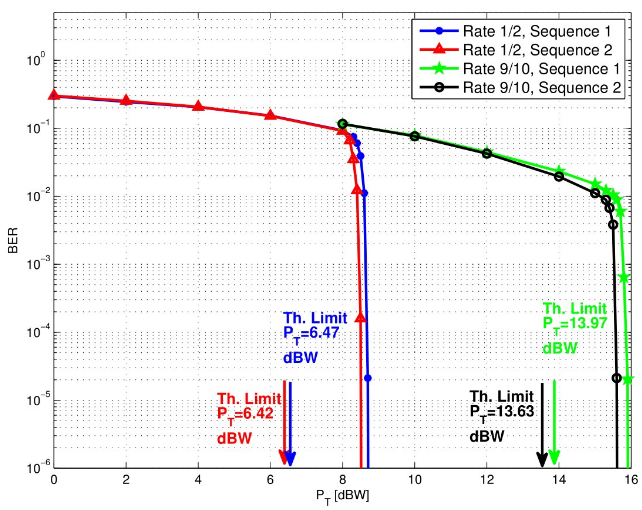


Figure 10. BER of OFDM for 16QAM, d=30 m, $M$=2, $N_R \times N_T = 10 \times 50$.

arrays; if we focus on the ratio between the ASE and the transceiver power consumption, namely on the system energy efficiency, optimal trade-off values for the transmit power and size of the antenna arrays should be found. These topics are certainly worth future investigation.

## REFERENCES

[1] J. G. Andrews, S. Buzzi, W. Choi, S. Hanly, A. Lozano, A. C. Soong, and J. C. Zhang, "What will 5G be?" *IEEE J. Select. Areas Commun.*, vol. 32, no. 6, Jun. 2014.

[2] A. Ghosh, T. A. Thomas, M. Cudak, R. Ratasuk, P. Moorut, F. W. Vook, T. Rappaport, J. G. R MacCartney, S. Sun, and S. Nie, "Millimeter wave enhanced local area systems: A high data rate approach for future wireless networks," *IEEE J. Select. Areas Commun.*, vol. 32, no. 6, pp. 1152 – 1163, Jun. 2014.

[3] T. S. Rappaport, S. Sun, R. Mayzus, H. Zhao, Y. Azar, K. Wang, G. N. Wong, J. K. Schulz, M. Samimi, and F. Gutierrez, "Millimeter wave mobile communications for 5G cellular: It will work!" *IEEE Access*, vol. 1, pp. 335–349, May 2013.

[4] T. S. Rappaport, F. Gutierrez, E. Ben-Dor, J. Murdock, Y. Qiao, and J. I. Tamir, "Broadband millimeter-wave propagation measurements and models using adaptive-beam antennas for outdoor urban cellular communications," *IEEE Trans. Antennas and Prop.*, vol. 61, no. 4, pp. 1850–1859, Apr. 2013.

[5] T. Bai, A. Alkhateeb, and R. Heath, "Coverage and capacity of millimeter-wave cellular networks," *IEEE Commun. Mag.*, vol. 52, no. 9, pp. 70–77, Sep. 2014.

[6] A. Alkhateeb, J. Mo, N. Gonzalez-Prelcic, and R. Heath, "MIMO precoding and combining solutions for millimeter-wave systems," *IEEE Commun. Mag.*, vol. 52, no. 12, pp. 122–131, Dec. 2014.

[7] V. Frascolla, M. Faerber, E. C. Strinati, L. Dussopt, V. Kotzsch, E. Ohlmer, M. Shariat, J. Putkonen, and G. Romano, "Mmwave use cases and prototyping: A way towards 5G standardization," in *Networks and Communications (EuCNC), 2015 European Conference on*, Jun. 2015, pp. 128–132.

[8] P. Banelli, S. Buzzi, G. Colavolpe, A. Modenini, F. Rusek, and A. Ugolini, "Modulation formats and waveforms for 5G networks: Who will be the heir of OFDM?" *IEEE Signal Processing Mag.*, vol. 31, no. 6, pp. 80–93, Nov. 2014.

[9] L. Deneire, B. Gyselinckx, and M. Engels, "Training sequence versus cyclic prefix-a new look on single carrier communication," *IEEE Communication Letters*, vol. 5, no. 7, pp. 292–294, Jul. 2001.

[10] M. Cudak *et al.*, "Moving towards mmwave-based beyond-4G (b-4G) technology," in *Proc. IEEE 77th VTC Spring*, Jun. 2013.

[11] S. Larew, T. Thomas, M. Cudak, and A. Ghosh, "Air interface design and ray tracing study for 5G millimeter wave communications," in *2013 IEEE Globecom Workshops*, Dec 2013, pp. 117–122.

[12] R. W. Heath, N. Gonzalez-Prelcic, S. Rangan, W. Roh, and A. Sayeed, "An overview of signal processing techniques for millimeter wave MIMO systems," *IEEE Journal of Selected Topics in Signal Processing*, vol. 10, no. 3, pp. 436–453, Feb. 2016.

[13] D. M. Arnold, H.-A. Loeliger, P. O. Vontobel, A. Kavčić, and W. Zeng, "Simulation-based computation of information rates for channels with memory," *IEEE Trans. Inform. Theory*, vol. 52, no. 8, pp. 3498–3508, Aug. 2006.

[14] A. Barbieri, D. Fertonani, and G. Colavolpe, "Time-frequency packing for linear modulations: spectral efficiency and practical detection schemes," *IEEE Transactions on Communications*, vol. 57, no. 10, pp. 2951–2959, Oct. 2009.

[15] S. Buzzi, C. Risi, and G. Colavolpe, "Green and fast DSL via joint processing of multiple lines and time-frequency packed modulation," *Physical Communication*, vol. 13, Part C, pp. 99 – 108, Dec. 2014.

[16] O. El Ayach, S. Rajagopal, S. Abu-Surra, Z. Pi, and R. Heath, "Spatially sparse precoding in millimeter wave MIMO systems," *IEEE Trans. on Wireless Commun.*, vol. 13, no. 3, pp. 1499–1513, Mar. 2014.

[17] S. Buzzi and C. D'Andrea, "On clustered statistical MIMO millimeter wave channel simulation," *Arxiv e-prints [online] Available: http://arxiv.org/pdf/1604.00648v2.pdf*, May 2016.

[18] S. M. Kay, *Fundamentals of statistical signal processing, Volume 1: Estimation theory*. Prentice-Hall, 1998.

[19] M. Iwanow, N. Vucic, M. Castaneda, J. Luo, W. Xu, and W. Utschick, "Some aspects on hybrid wideband transceiver design for mmwave communication systems," *Proc. of 20th International ITG Workshop on Smart Antennas (WSA 2016)*, Jun. 2016.

[20] H. Ghauch, T. Kim, M. Bengtsson, and M. Skoglund, "Subspace estimation and decomposition for large millimeter-wave MIMO systems," *IEEE Journal of Selected Topics in Signal Processing*, vol. 10, no. 3, pp. 528–542, Apr. 2016.